MATERIALS CHEMISTRY FRONTIERS

A Defect Electrocatalytic Mechanism: Concept, Topological Structure and Perspective

Journal:	*Materials Chemistry Frontiers*
Manuscript ID	QM-REV-02-2018-000070.R1
Article Type:	Review Article
Date Submitted by the Author:	23-Mar-2018
Complete List of Authors:	Jia, Yi; Griffith University, Queensland Micro and Nanotechnology Centre Chen, Jun; Intelligent Polymer Research Institute, Chemistry Yao, Xiangdong; Griffith University, Queensland Micro and Nanotechnology Centre

MATERIALS CHEMISTRY FRONTIERS

REVIEW

A Defect Electrocatalytic Mechanism: Concept, Topological Structure and Perspective

Received 00th January 20xx,
Accepted 00th January 20xx

DOI: 10.1039/x0xx00000x

www.rsc.org/

Yi Jia,[a] Jun Chen*[b] and Xiangdong Yao*[a]

Carbon-based materials have been attracting numerous interests for electrocatalysis due to various merits such as abundance, low cost, high conductivity and tunable molecular structures. However, to date, the electrochemical activities of these electrocatalysts are mainly attributed to different active dopants (e.g., N, B, P or S), leading to a common concept that heteroatom doping is essential for carbon based electrocatalysts. Recently, we present a new concept that the specific topological defects can activate the oxygen reduction reaction (ORR) and develop a facile method to create such unique defects. Subsequent research extends this new mechanism to other reactions such as hydrogen and oxygen evolution (HER and OER) and confirms that heteroatom doping is not essential but these defects can serve as actives sites for electrochemical reactions. This new theory then creates a new research direction in electrocatalysis. In this short review, we will summarise the origin and presentation of defect mechanism concept, the possible topological defect structures that are effective for electrochemical reactions, the formation of desirable defects, the challenges on synthesis and characterization of typical defects, and future research directions on electrochemical defect mechanism.

1. Introduction

Owing to the energy crisis and environmental issues, it is imperative to develop the clean energy technologies in a sustainable fashion for the next decades. Various advanced technologies for renewable energy conversion and storage, such as water electrolysis, electrochemical production of hydrogen peroxide, regenerative fuel cells and rechargeable metal-air batteries, have generated great expectations through both fundamental and applied studies.[1-7] The core of these renewable energy technologies involves a series of electrochemical processes, for example, hydrogen evolution reaction (HER) and oxygen evolution reaction (OER) at the cathode and the anode of a electrochemical water-splitting cell, and oxygen reduction (ORR) and oxygen evolution (OER) at the air electrodes of regenerative fuel cells and rechargeable metal-air batteries.[4,6,7] In fact, energy conversion in electrochemical processes is often hindered by high activation energy barriers, which needs extra energy to overcome. The extent of the barrier is defined by overpotential or faradic efficiency.[8,9] Therefore, electrocatalysts are always applied to improve the performance of electrode, in order to lower activation energy and increase conversion rate. In this regard, the performance of the electrocatalyst as a key aspect is paramount to the properties of an electrochemical system (e.g. energy efficiency, conversion rate, lifetime and cost). However, the current scope of catalysts utilized for these fundamental electrochemical reactions is dominated by precious metal-based materials, such as platinum (Pt) based catalyst for ORR/HER, iridium (Ir) and ruthenium (Ru)-based catalysts for applications in OER.[6,7] Their 'rare earth' status and associated high cost renders them less than ideal materials for incorporation into bulk production scale that will be required for aforementioned clean energy conversion devices. In recent years, a wide variety of transition metals (Co, Ni, Fe, Mo) based materials have been developed as effective nonprecious electrocatalysts, however, the inherent corrosion and oxidation susceptibility largely limits their utilization in acidic proton-exchange membrane-based electrochemical devices.[2,10-26] Therefore, new strategies are highly desirable to develop efficient electrocatalysts and/or improve the electrocatalytic activity and stability of existing materials.

Carbon-based materials feature unique advantages for designated catalysis due to their tunable molecular structures, abundance, and robust tolerance to acidic/alkaline conditions.[4,5,27-34] Considerable research efforts have been devoted to making carbon-based materials as a new class of electrocatalysts for fundamental electrochemical reactions (ORR, OER and HER) by heteroatoms doping engineering (e.g. N, B, P and S), and several excellent reviews relevant to this topic are available.[4,7,31-33] Besides application in electrocatalysis, such carbon based catalysts (e.g. carbon nitrides and carbon-doped boron nitrides) can also be the promising candidates in wider applications such as photocatalysis[35-38], oxidative dehydrogenation of alkane.[39,40,41] and supercapacitor[42-44]. Recent studies demonstrate that the electrocatalytic activities

[a] School of Natural Sciences and Queensland Micro- and Nanotechnology Centre, Griffith University, Nathan campus, QLD 4111, Australia. E-mail: x.yao@griffith.edu.au
[b] Intelligent Polymer Research Institute, ARC Centre of Excellence for Electromaterials Science, AIIM Facility, Innovation Campus, University of Wollongong, Wollongong, NSW 2522, Australia. E-mail: junc@uow.edu.au

of heteroatom-doped carbon materials originate from activating carbon π electrons by breaking the integrity of π conjugation.[45-47] With this understanding, it is intuitive to consider that the intrinsic/induced defects in sp^2 carbon could also break the integrity of π conjugation to enhance the electrocatalytic activities. Most recently, our group and other peers demonstrate that the specific carbon defects play as the active sites for electrochemical reactions (ORR, OER and HER). To date, the research and development of defective electrocatalysts is still in the very early stages, and further mechanistic studies are urgently desirable.

This short review provides an overview of this newly developing field in defective electrocatalysis, including the origin of defect mechanism and the defect topologies that are possible active sites for the reactions. It is also gained mechanistic understanding on correlations between electronic structures of defective carbon based materials and electrocatalysis. A special emphasis is placed on the defect catalysis mechanism originating from both defect types (analogous to n or p type behavior for specific electrochemical reactions) and defect density, which may provide the guidance to atomic design of highly active electrocatalysts for diverse applications in energy conversion and storage. Finally, we briefly point out the current challenges and propose the opportunities facing this burgeoning field.

2. Account of recent work on defective carbon based materials for advanced electrocatalysis

The defect engineering in carbon based materials is of growing importance for optimizing the electrocatalytic activities of fuel cell (ORR) and water splitting (OER and HER) relevant reactions. In this section, we showcase the progress of defective carbon based materials for electrocatalysis (Fig. 1). Firstly, we introduce the concept of defect electrocatalysis, including how this defect mechanism for ORR has been discovered,[48] in which we clearly presented the concept of defect mechanism, exhibited the topological defect (e.g. the combination of carbon rings with pentagon-octagon-pentagon, denoted as D585) as the active sites and developed a methodology to create such defects for ORR. Almost in the meantime, Xia and co-workers theoretically studied the effect of different defect types in graphene on the ORR activities using density functional theory (DFT) methods.[90] Then, we present controllable strategies in preparing diverse carbon materials with defects.[48-56] Importantly, the defective carbon based materials exhibit excellent ORR activities, which overcomes the common sense of the necessity of heteroatom doping.[49] Besides carbon defect mechanism for ORR, our group further demonstrates defects as active sites in carbon (graphene used as an ideal model material for direct instrumental identification purpose) are also functional for other electrochemical reactions such as OER and HER, which may originate from different types of carbon defects.[52] Moreover, the defects are those high-energy sites that can interact strongly with the metallic nanoparticles/species. This feature may provide good opportunities to significantly

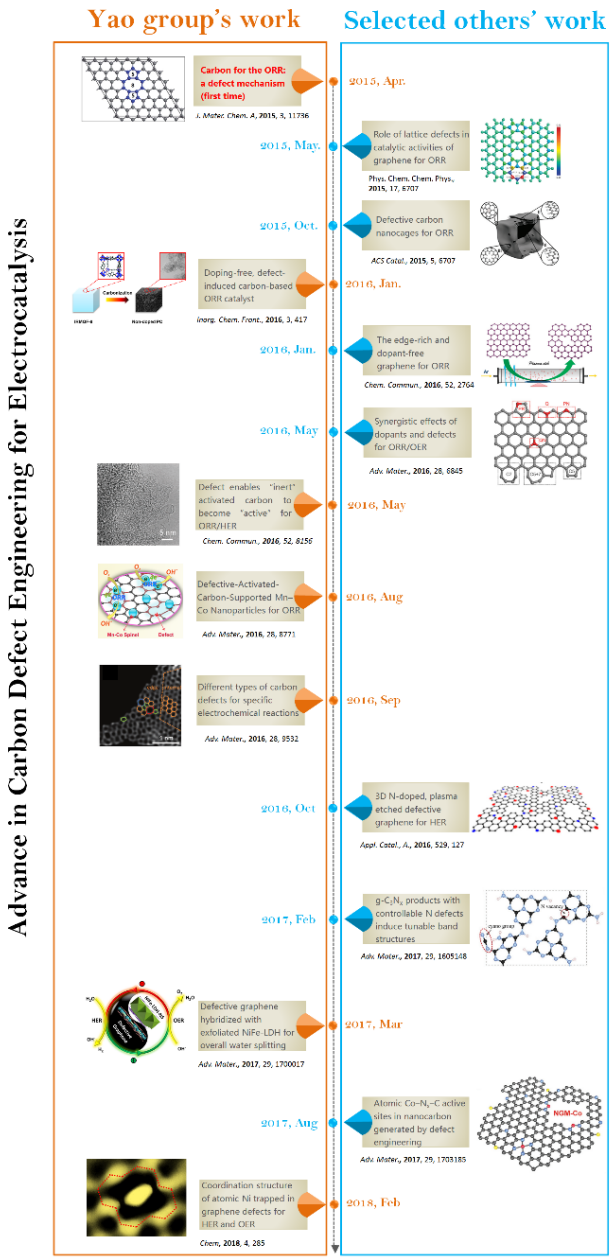

Fig. 1 Timeline showing the significant advance in carbon defect research for electrocatalysis.

enhance the catalytic activity and catalyst durability.[52,57-61] The defects on carbons for electrocatalysis is emerging, and the simultaneous and subsequent research from other groups is also discussed.

2.1 Investigations of N-ORR activity relationship

Nitrogen doping on carbon nanotubes array was found to be functional for oxygen reduction reaction (ORR) dating back to 2009.[27] Generally, the improved ORR activity is attributed to the doping-induced charge redistribution, which is appealing to oxygen molecule adsorption and dissociation.[4,31,62,63] Since the nitrogen dopants present four dominant types, including pyridinic nitrogen, pyrrolic nitrogen, graphitic nitrogen and

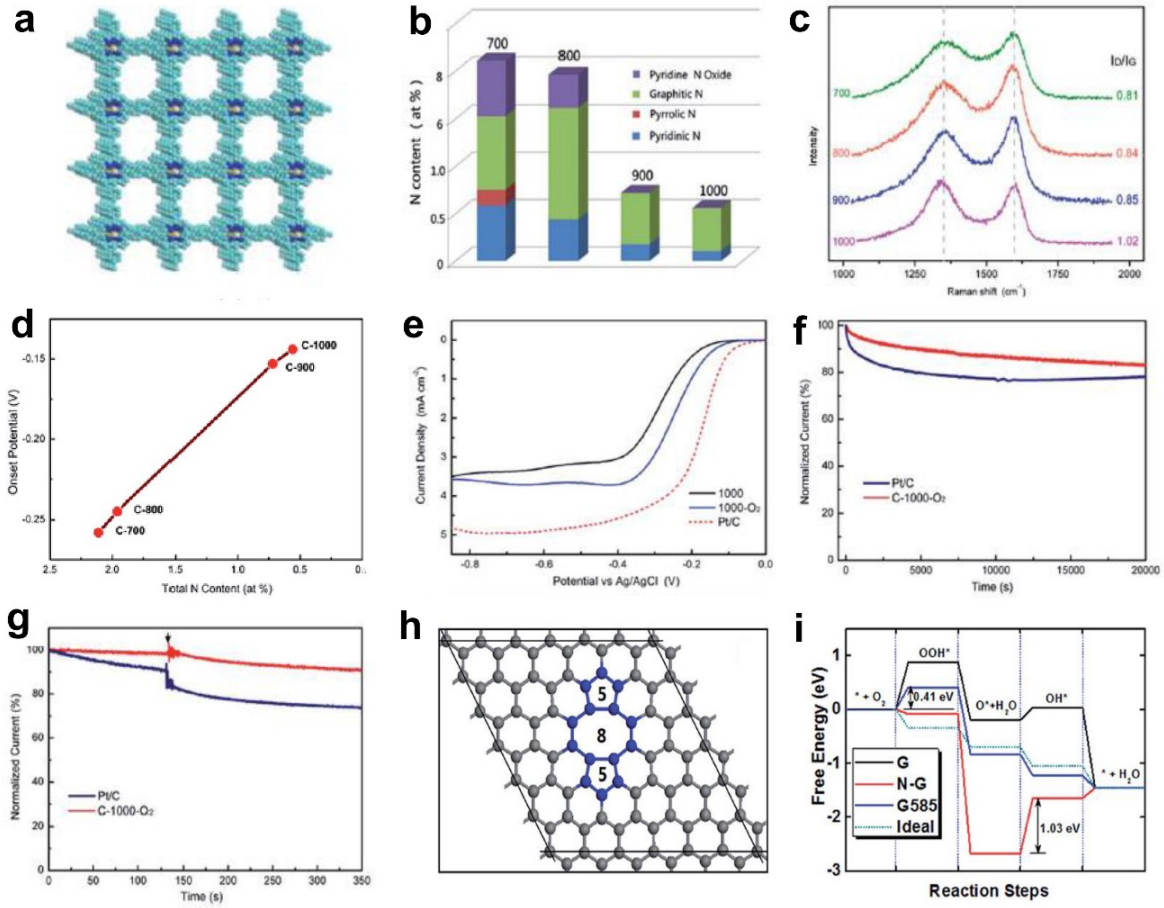

Fig. 2 Investigations of N-ORR activity relationship and the corresponding defect mechanism study. a) Schematic of a N-enriched porous aromatic framework material (PAF-40), which is a precursor to synthesize defective carbon. b-d) Relative atomic percentage of different nitrogen bonding states, Raman spectra and ORR onset potentials in prepared defective carbons treated under a temperate range (700 °C, 800 °C, 900 °C and 1000 °C). e) ORR polarization curves of C-1000, C-1000-O_2 and Pt/C recorded at room temperature in an O_2-saturated 0.1 M KOH electrolyte. f and g) Stability test and methanol tolerance test of C-1000-O_2 and Pt/C. h) Atomic structure of G585 defect in graphene. i) N-doped graphene (N-G), graphene with G585 defects (G585) and an ideal catalyst (Ideal) for ORR at the equilibrium potentials. Reproduced with permission.[48] Copyright 2015, RSC.

oxidized nitrogen, many attentions have been devoted into exploiting the actual active site of nitrogen doped nanocarbons for ORR. Currently, the debate of N active site is mainly focused on two mainstream perspectives. One suggests that pyridinic nitrogen is the active site for ORR.[64-71] Particularly, an article in the prestigious journal *Science* investigated the active sites through a controllable synthesis of specific types of nitrogen dopants in a highly oriented pyrolitic graphite (HOPG).[71] It is reported that the pyridinic nitrogen plays the essential role for ORR due to creating Lewis basic sites and activating the adjacent carbon atoms.[71] The other indicates the graphitic nitrogen is the active sites for ORR, which is also supported by both theoretical and experimental studies.[72-77] In addition, specific type of N dopant is also proved to be active to oxygen evolution reaction (OER) and hydrogen evolution reaction (HER). For instance, Lei and co-workers demonstrated that carbon catalyst with rich oxidized nitrogen exhibited a higher activity in water splitting than those with abundant pyridinic nitrogen, pyrrolic nitrogen and graphitic nitrogen, implying that the oxidized nitrogen may be the potential active site for HER and OER.[78] Under the direction of the N-doping mechanism, massive research interests have been focused on increasing the N-doped amount in carbons in order to further elevate their ORR properties.[79-85] Interestingly, by summarizing the reported data on correlations of N concentration for N-doped carbon based eletrocatalysts and their ORR activity from literatures,[79-85] it is presented a diverse and non-positive correlation, which is not fully consistent with the N-doping mechanism. Such a discordancy in N-ORR activity relationship may be attributed to the following two aspects: (1) the deterioration of the electronic conductivity due to excessive N-doping amount, which destructs the perfect sp^2 carbon lattice; (2) besides N-doping effect, there may be also something else in leading to overall ORR property. Thus, it is very essential to get in-depth insight into the N-ORR activity relationship.

Recently, Yao group investigated the correlation between catalytic activity of N-doped systems and the nitrogen content

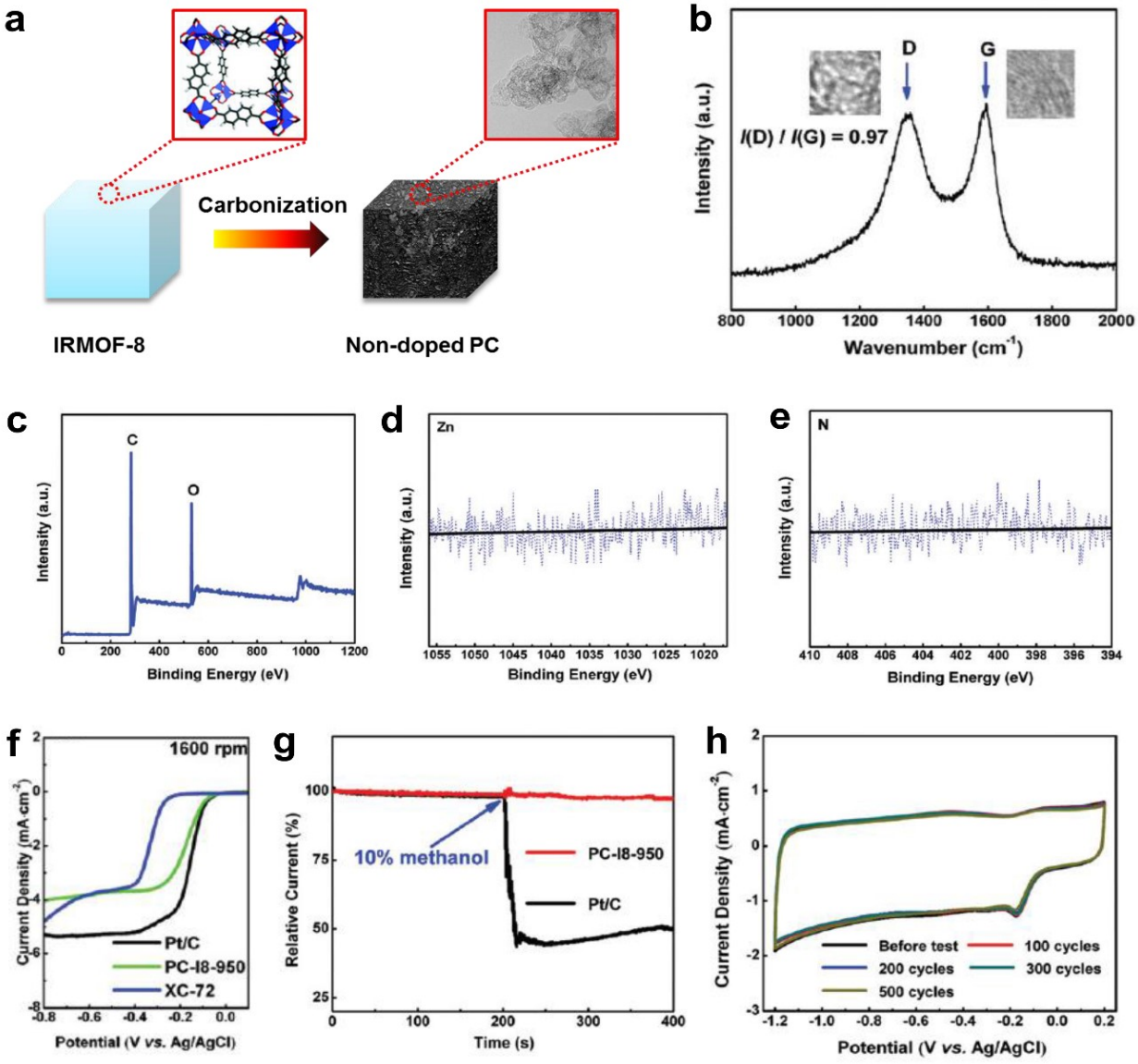

Fig. 3 Investigation of ORR activity in non-doped porous carbon (PC) derived from IRMOF-8 carbonization. a) Schematic structural changes of IRMOF-8 with carbonization to yield non-doped PC. b-e) Raman spectrum, XPS survey spectrum and high resolution XPS spectra (Zn 2p and N 1s) of non-doped PC, respectively. f) LSV curves at 1600 rpm of non-doped PC, Pt/C and XC-72 catalysts. g) Chronoamperometric stability and methanol tolerance tests of non-doped PC and Pt/C. h) CV stability test of non-doped PC up to 500 cycles with a scanned rate of 50 mV s^{-1}. Reproduced with permission.[49] Copyright 2016, RSC.

in the ORR by carbonization of a N-enriched porous organic framework material (PAF-40) with 12.14 atom % N (Fig. 2a).[48] It is notable that the N contents decrease stepwise with the increase of the calcination temperatures (Fig. 2b). In contrast, Raman spectra (Fig. 2c) illustrate that I_D/I_G ratio increasing from 0.81 to 1.02 with the ascending carbonization temperatures, suggesting a higher disordering degree of sp^2 carbon lattice due to induced carbon defects in prepared samples at higher temperatures. Unexpectedly, in ORR linear sweep voltammetry (LSV) tests (Fig. 2d), it is observed an inverse relationship between N-content of the sample and catalytic activity, i.e. the lower the nitrogen content the higher the ORR activity in a nitrogen range of 0.56~2.11 atom % N (negative correlation of the relationship). Furthermore, to exclude the effect of temperature on carbon structure that may influence the ORR activity, a controlled experiment has been performed. The materials were prepared at the same temperature of 1000 °C, but a trace of O_2 was introduced to the protecting gas Ar, aiming to help for further removal of N. Thus a lower N content of 0.21 atom% was obtained and the sample exhibited much higher activity than the sample of 0.56 atom% N (Fig. 2e-g). All these results clearly imply that besides general N-doping effect, the removal of N atoms from sp^2 carbon lattice could create valuable defects, which is possible to contribute to the higher ORR activity. After searching for various topological defects on graphene, we found that the stable divacancy (DV) defect (e.g.

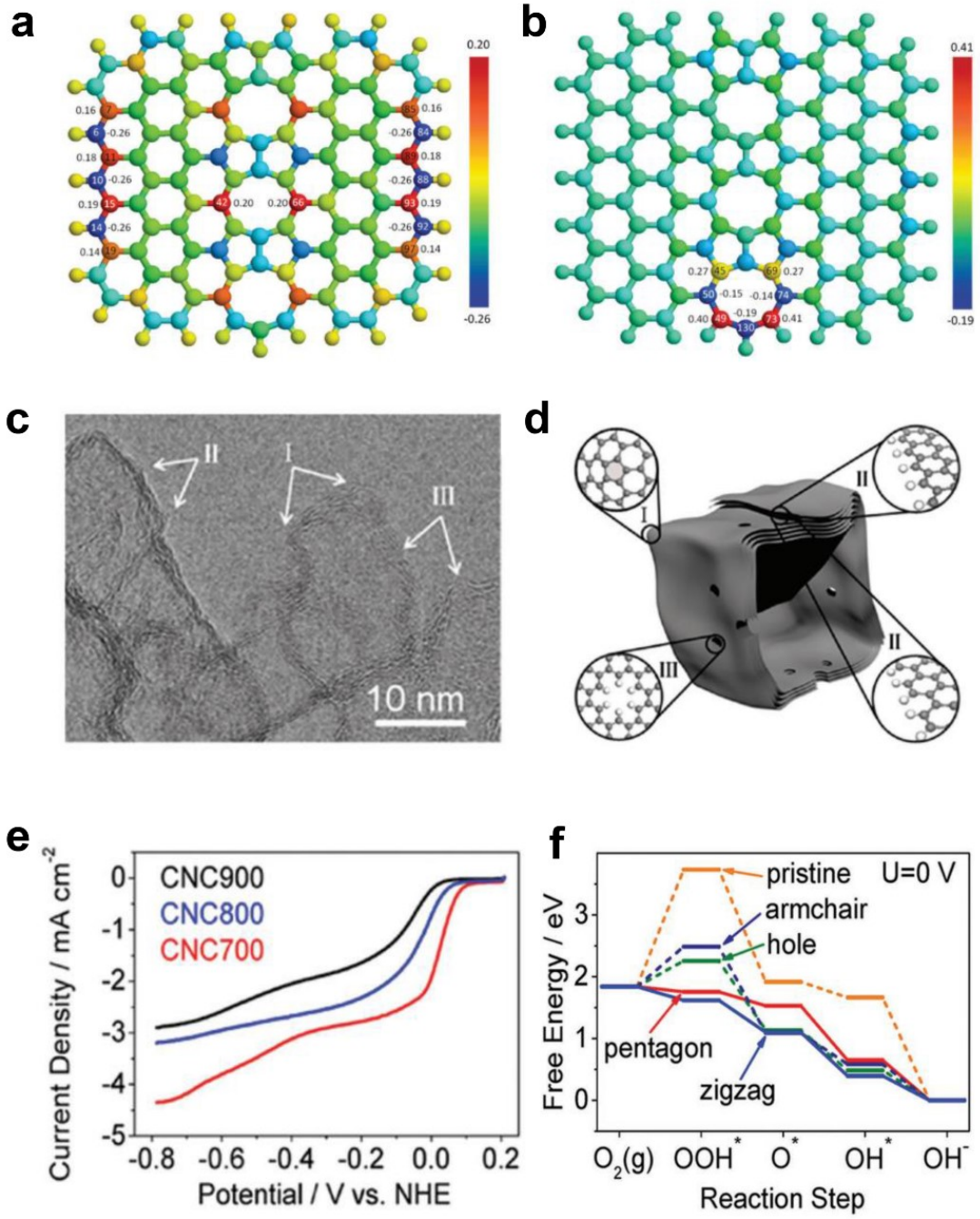

Fig. 4 a) Charge and b) spin density distributions on the graphene cluster containing a line defect with an odd number of octagon and fused pentagon carbon rings. Reproduced with permission.[90] Copyright 2015, Royal Society of Chemistry. c) HRTEM image of CNC700. d) Schematic structural character of the carbon nanocages. I, II, and III in the highlighted diagrams represent three typical defect locations. e) ORR performances of CNC700, CNC800, and CNC900 in O_2-saturated 0.1 M KOH. f) Free energy diagrams for ORR activities of different defects in CNC700. Reproduced with permission.[53] Copyright 2015, American Chemical Society.

G585),[86,87] might be effective to activate the ORR. As shown in Fig. 2h, density functional theory (DFT) calculations reveal that G585 defects are active and comparable to Pt in all steps for ORR (close to the ideal catalyst as shown in Fig. 2i). To our best knowledge, it is the first time to prove a defect mechanism in ORR by using defective carbon. Although the proposed defects (G585) have not been directly observed and residual N (0.21 atom % N) cannot be completely eliminated in our optimal defective carbon at this early stage, the newly presented defect mechanism may open a new window to direct the proof-of-

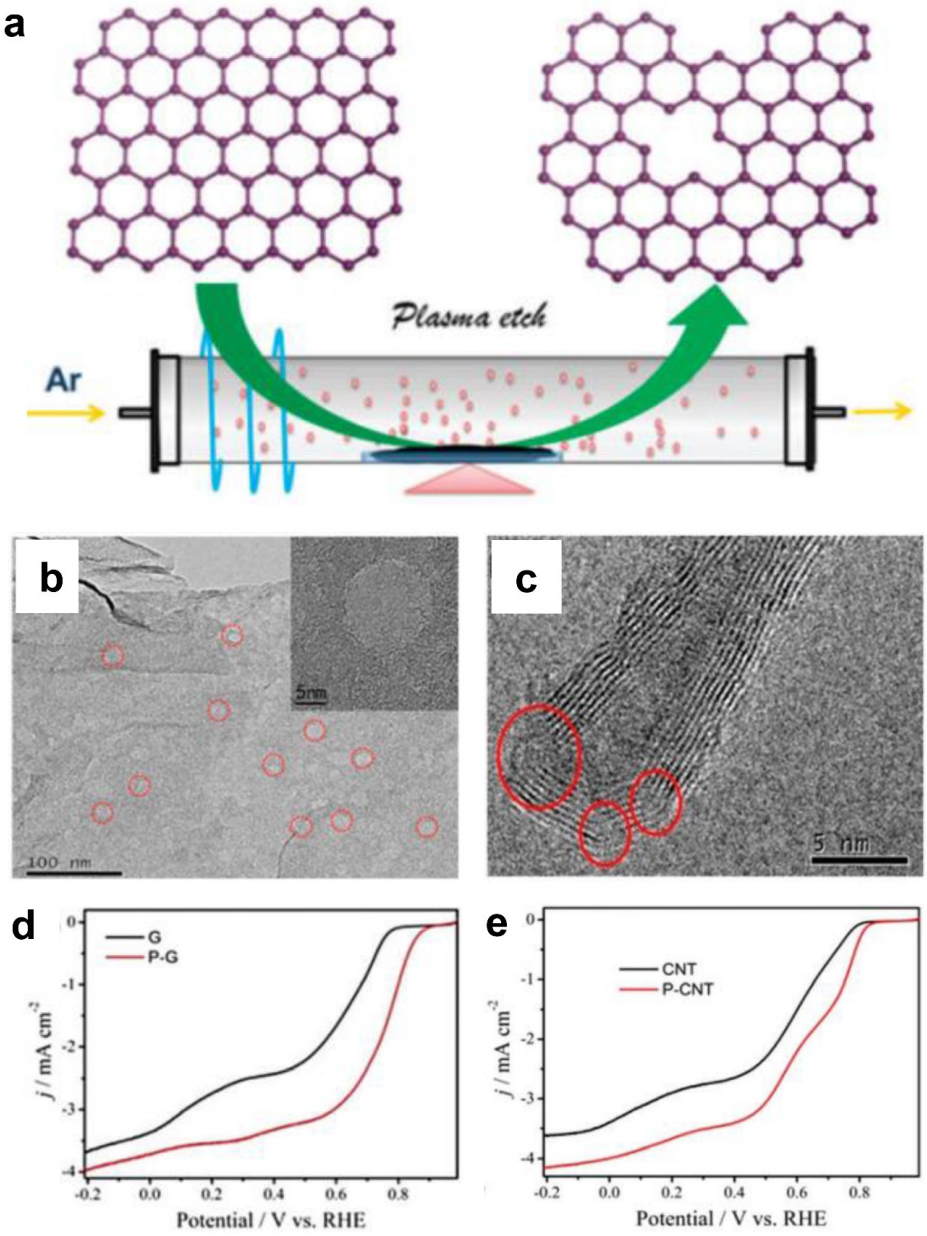

Fig. 5 a) Illustration of the preparation of the defective graphene by Ar plasma etching. TEM images of b) Ar plasma-treated graphene and c) carbon nanotube. d) ORR performances of pristine and Ar plasma treated defective graphenes in O_2-saturated 0.1 M KOH. e) ORR performances of pristine and Ar plasma treated defective carbon nanotubes in O_2-saturated 0.1 M KOH. Reproduced with permission.[54] Copyright 2015, RSC.

concept atomic design of highly active non-metal electrocatalysts.

2.2 ORR activity in defective carbons

To completely eliminate the N effect in defective carbon based materials for electrocatalysis, our group subsequently carbonized a Zn-metal organic framework material (IRMOF-8) by removing all of the Zn to yield a derived carbon containing only C and O, without any active doping elements (e.g., N, B, P or S) as determined by X-ray photoelectron spectroscopy (XPS).[49] Fig. 3a presents the schematic structural changes of IRMOF-8 with carbonization to yield non-doped porous carbon (PC) as a black soot-like material, which is in a similar method to processes reported previously.[88,89] Raman spectrum (Fig. 2b) illustrates the disorder structure and the multilayer/graphitic stacked domains in the derived carbon framework. Importantly, successful synthesis of non-doped porous carbon (PC) is firmly evidenced by XPS spectra without presence of Zn 2p and N 1s traces (Fig. 2c-e). To experimentally authenticate the proof-of-concept of the defect catalytic mechanism in ORR, the LSV

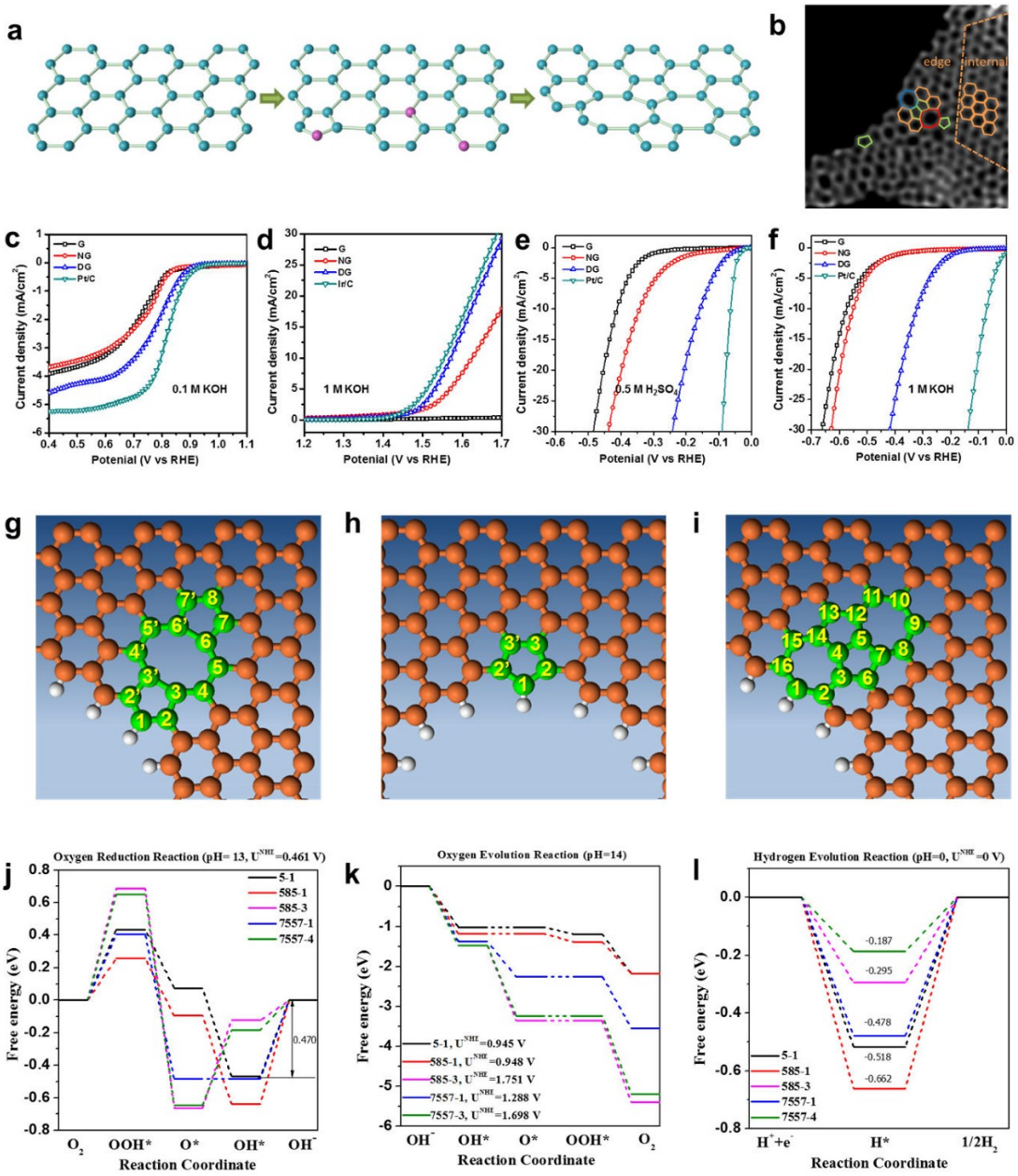

Fig. 6 a) The schematic of the formation of DG. b) HAADF image of DG with an acceleration voltage of 80 kV. Hexagons, pentagons, heptagons, and octagons were labelled in orange, green, blue, and red, respectively. c-f) Linear sweeping voltammetry curves of the pristine graphene, NG, and DG. c) Oxygen reduction reaction. d) Oxygen evolution reaction. e) Hydrogen evolution reaction in acid and f) alkaline solution, respectively. g-l) Mechanism study of trifunctionality in defective graphene for ORR, OER, and HER. g) D585 defect. h) Edge pentagon. i) D7557 defect. j–l) Schematic energy profiles for the ORR pathway, the OER pathway, and the HER pathway on defective graphene in alkaline/acidic media. To improve legibility, "OH–" was omitted from the labels. Reproduced with permission.[50] Copyright 2016, Wiley-VCH.

measurements were carried out. As expected, the derived pure defective carbon exhibited excellent ORR activity (Fig. 2f), in contrast to the requirements of the heteroatom doping mechanism (that is no doping, no activity). Moreover, this defective carbon material demonstrates the improved molecular selectivity and stability as compared to commercial Pt/C catalyst (Fig. 2g and h).

Our preceding findings demonstrate the critical role of defects of carbon, that is, carbon materials with more defects have better activities than pristine carbon (and even doped carbons).[48,49] Researchers from other groups also started to

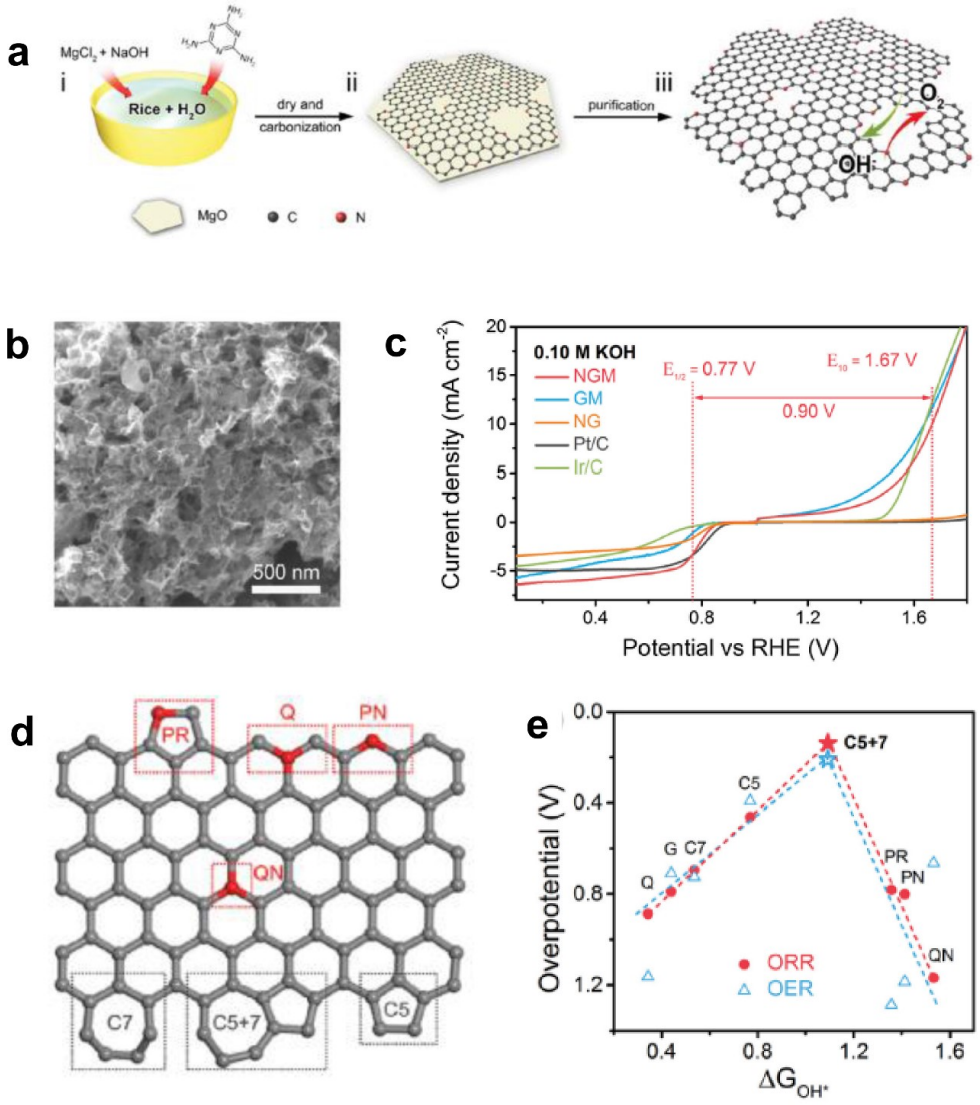

Fig. 7 a) Schematic of the fabrication of a unique niintettrogen-doped and edge-rich 3D graphene (nitrogen-doped mesh, denotes as NGM). b) TEM image showing the interconnected nanoplates of NGM. c) ORR/OER bifunctional activities of NGM, GM, NG, commercial Pt/C and Ir/C catalysts. d) A schematic graphene nanoribbon with different kinds of N-doping or topological defects (PR: pyrrolic nitrogen; PN: pyridinic nitrogen; Q: quaternary nitrogen on the edge; QN: quaternary nitrogen in the bulk phase; C5: five-carbon ring; C7: seven-carbon ring; C5+7: five-carbon ring adjacent to seven-carbon ring). e) ORR and OER volcano plots of overpotential versus adsorption energy of OH*, indicating the C5+7 as the optimal active site for both ORR and OER electrocatalysis. Reproduced with permission.[51] Copyright 2016, Wiley-VCH.

devote great efforts to prepare carbon based materials with a large number of intrinsic/induced defects. Almost simultaneously, Xia and co-workers theoretically studied the effect of point- and line-defect in graphene on the catalytic activities using density functional theory (DFT) methods.[88] Particularly, they found that pentagon ring at the zigzag edge and the line-defect pentagon–pentagon–octagon chain significantly modified local charge/spin polarization at the defective sites, leading to catalyze ORR (Fig. 4a and b).[90] They further claimed that reaction energy barriers of the four-electron transfer pathway on defective graphene are comparable to that of platinum.[90] Experimentally, Hu and co-workers used purely defective carbon nanocages (CNCs) with high specific surface area (SSA), which contains abundant holes and edges but without any dopants to address the influence of intrinsic carbon defects on ORR activity (Fig. 4c-e).[53] It is noteworthy that the CNC700 with the highest defect level (I_D/I_G ratio in Raman spectrum is 2.29) exhibited the best ORR activity with a high onset potential about 0.11 V vs normal hydrogen electrode (NHE) in 0.1 M KOH (Fig. 4e). The electron transfer number (n) and the corresponding peroxide species (HO_2^-) are further calculated to be ~2.90 ± 0.10 and ~55%, respectively,

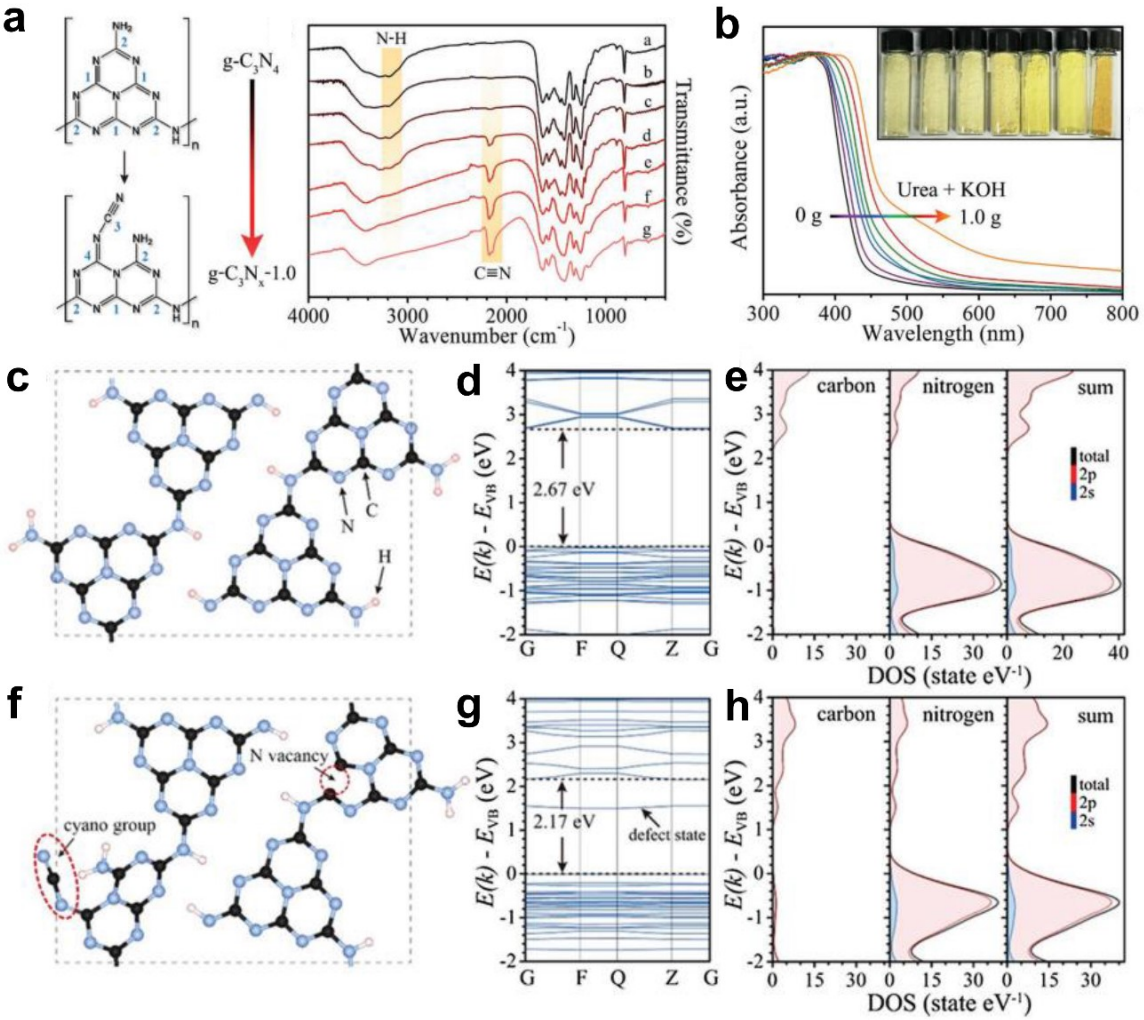

Fig. 8 a) FTIR spectra of g-C_3N_4 and g-C_3N_x with proposed structure changes in heptazine units before and after introducing cyano groups. b) UV–vis diffuse reflectance spectra (DRS) for g-C_3N_4 and g-C_3N_x prepared using urea as precursor and different amounts of KOH (ranging from 0 to 1.0 g). c) and f) Structure models of g-C_3N_4 and g-C_3N_x with N defects (including –C≡N group and N vacancy). d) and g) Calculated band structures. e) and h) Corresponding partial density of states (PDOS) for g-C_3N_4 and g-C_3N_x, respectively.[56] Copyright 2017, Wiley-VCH.

suggesting a mixed two-electron and four-electron process. Remarkably, the comparison experiments showed that the defective CNC700 is even superior to N/B-doped CNTs in ORR, which clearly indicates the significant contribution of the carbon defects in electrocatalysis. DFT calculations indicate that the pentagon and zigzag edge defects are responsible for the high ORR activity in defective CNCs, which is attributed to the redistributed electronic structures from unpaired π electrons at carbon defects sites (Fig. 4f).[53]

Alternatively, Wang and co-workers used Ar plasma method to etch the surface of graphene and carbon nanotubes (CNTs) to expose plenty of defects on the perfect carbon lattice (Fig. 5a).[54] TEM images illustrated that massive holes and cracks existed in Ar plasma treated defective graphene and CNTs, respectively (Fig. 5b and c), suggesting the level of defects increased due to the additional exposed edges. The ORR performances of Ar plasma treated defective graphene and CNTs were both enhanced as compared to the pristine counterparts (Fig. 5d and e), which are ascribed to formed defects playing the active sites for ORR electrolysis. These findings on defective carbons may push us to reconsider the origin of the improved ORR activity for carbon based materials.[54]

2.3 Defective graphene: defect mechanism for ORR, OER and HER

As discussed in Section 2.1 and 2.2, a defect catalytic mechanism in ORR was proved by both experimental results and theoretical calculations. However, currently a few issues

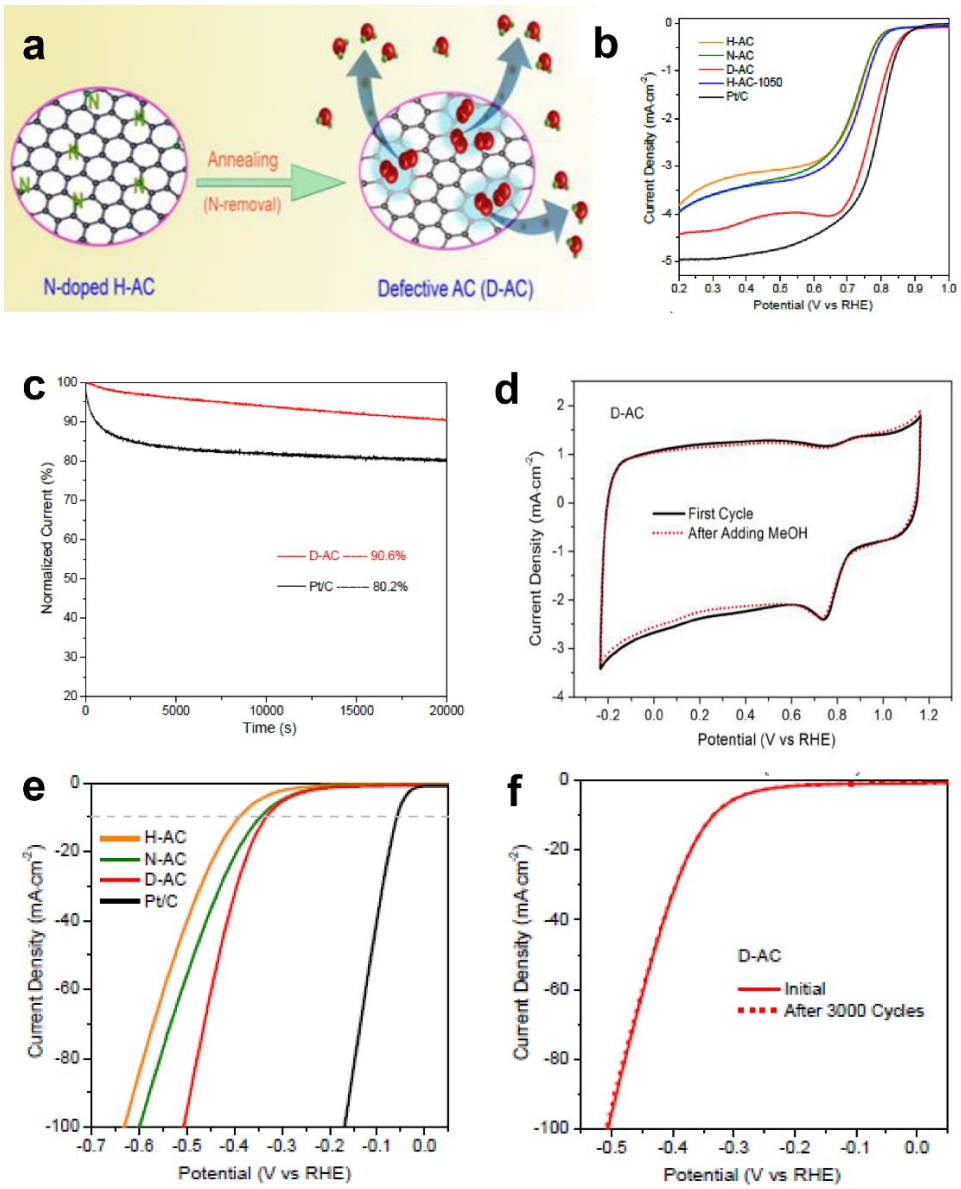

Fig. 9 a) The schematic of the formation of defective activated carbon (D-AC) for enhancing ORR performance. b) LSV curves of the H-AC, N-AC, D-AC and Pt/C measured at the rotation speed of 1600 rpm in O_2-saturated 0.1 M KOH solution. c) Amperometric i-t curves of the D-AC and Pt/C. d) Rotation ring-disk electrode voltammogram of the H-AC, D-AC and Pt/C in O_2-saturated 0.1 M KOH solution at 1600 rpm. e) HER polarization curves of the H-AC, N-AC, D-AC and Pt/C measured at the scan rate of 10 mV s^{-1} in 0.5 M H_2SO_4 solution. f) HER polarization curves recorded for the D-AC before and after 3000 cycles of CV scan under acidic condition. Reproduced with permission.[52] Copyright 2016, RSC.

are still considered to be addressed for understanding the defect catalytic mechanism: (i) the topological defects such as in PAF/MOF derived carbons have not been directly observed due to resulting complex 3D structures obtained after carbonization;[48,49] (ii) according to theoretical correlations of carbon defect types and electronic structures, carbon defects can be analogously categorized into n-type and p-type, leading to potential enhancement in electrochemical reductions (e.g. ORR and HER) and oxidation reactions (e.g. OER), respectively.[91-93] Although defect catalysis has been explored in ORR, whether defective carbons possessing multi-types of defects are also functional for other electrochemical reactions such as OER and HER still is unknown.

To tackle these issues, our group developed the 2D defective graphene (DG) obtained via a facile nitrogen removal procedure from a N-doped precursor (Fig. 6a).[50] As the synthetic process may create different types of defects, the aberration-corrected high-resolution transmission electron microscopy (AC-HRTEM) was used to actually visualize the defects regions of the material. Strong lattice disorder can be witnessed near the edge

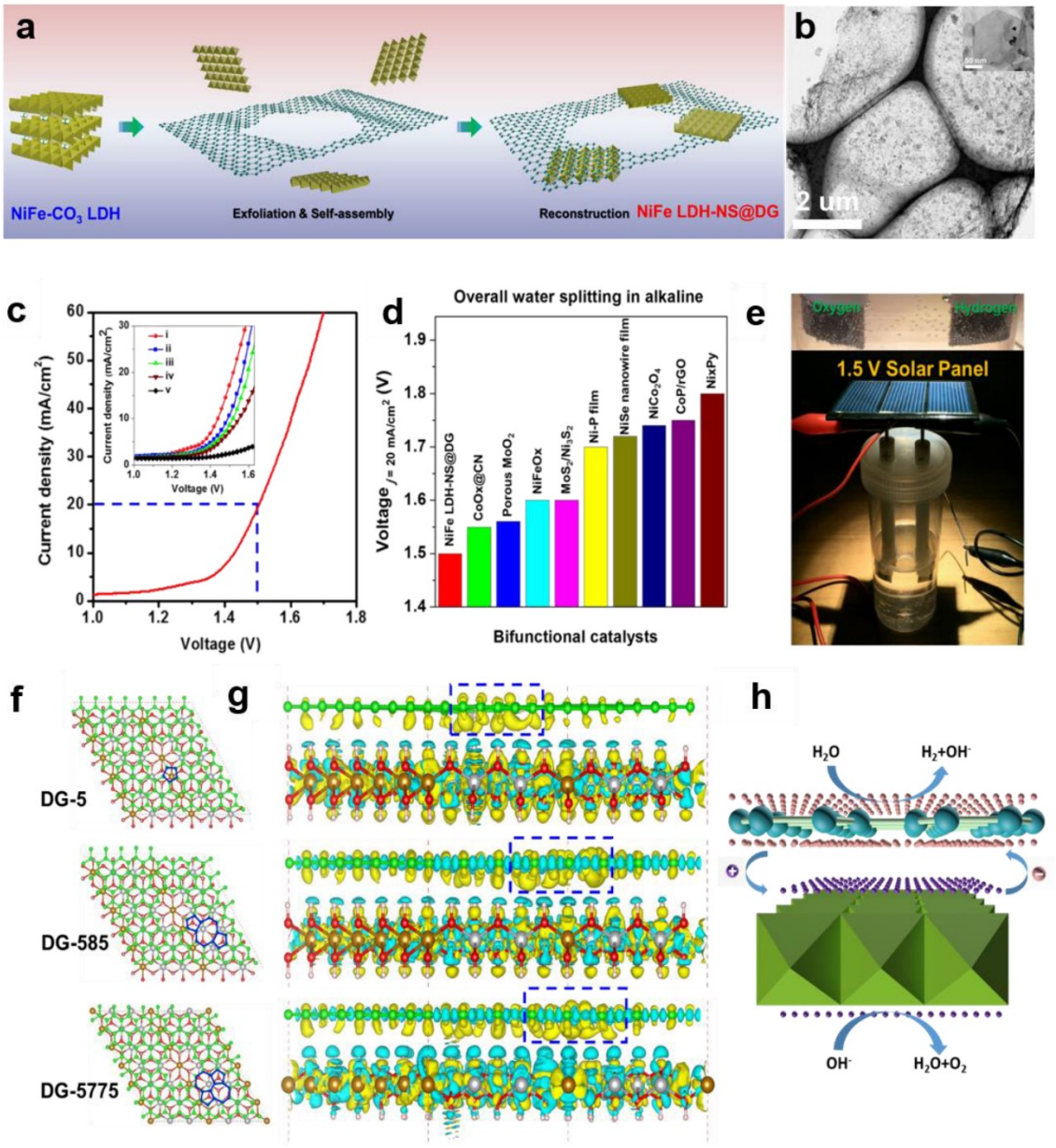

Fig. 10 a) Schematic illustration of the preparation of NiFe LDH-NS@DG nanocomposite and b) its TEM images with low and high (inset) magnifications. c) Linear sweeping voltammetry curve of NiFe LDH-NS@DG10 as OER and HER bifunctional catalyst in 1 M KOH for overall water splitting (both loaded into Ni foam at a loading of 2 mg cm^{-2}), with the inset showing comparison of different catalysts including (i) NiFe LDH-NS@DG10 with 2 mg cm^{-2} loading; (ii) NiFe LDH-NS@DG10 with 1 mg cm^{-2} loading; (iii) NiFe LDH-NS@NG10 with 2 mg cm^{-2} loading; (iv) NiFe LDH-NS@ G10 with 2 mg cm^{-2} loading; (v) bare Ni foam electrode). d) Comparison of the required voltage at a current density of 20 mA cm^{-2} for the NiFe LDH-NS@DG catalyst with other state-of-the-art noble metal free bifunctional catalysts. e) Demonstration of a solar power assisted water-splitting device with a voltage of 1.5 V. f-g) DFT calculation studies of Ni–Fe LDH-NS@DG (DG-5, DG-585, or DG-7557) based composite. Yellow and cyan isosurfaces represent charge accumulation and depletion in the 3D space with an isosurface value of 0.002 e $Å^{-3}$. h) The schematic of the probable electrocatalytic mechanism of Ni–Fe LDH-NS@DG for HER and OER is presented based on the DFT calculation results. Reproduced with permission.[58] Copyright 2017, Wiley-VCH.

of the graphene sheet (Fig. 6b), which can be attributed to the various structural defects marked in the image. Afterward, the evaluation of the electrocatalytic activities demonstrated that the DG material is functional not only for the ORR but also for

the OER and HER, and the activity of the material is significantly higher than that of the parent NG for all the three basic electrochemical reactions (Fig. 6c-f). To get the in-depth insight of the underlying catalytic mechanisms, density function theory (DFT) calculations of the reaction energy profiles towards HER, OER and ORR were conducted. Three computational models were built based on the AC-HRTEM observed types of defects in the DG material, i.e., edge pentagon, D585 and D7557 (the combination of carbon rings with heptagon-pentagon-pentagon-heptagon) (Fig. 6g-i). Remarkably, the energy profiles for ORR, OER, and HER (Fig. 6j-l) reveal that active sites for different electrochemical reactions are induced by specific defect types due to particular desired reactant binding energy for each electrochemical reaction. It should be noted that in all cases, the defective graphene is superior to N-doped graphene for ORR, HER and OER. It is speculated that the activity of N-doped graphene is also from the vacancy type defects as the doping process is dynamic with some N release as well to create the vacancies. Due to the much lower density of available vacancies, the activity is lower.

Recently, Zhang and co-workers demonstrated the enhancement in reaction pathway of ORR/OER through both experimentally electrochemical evaluation and theoretical calculations by using a unique nitrogen-doped (7.60 atom %) and edge-rich 3D graphene model system obtained via the carbonization (950 ^{o}C under Ar) of sticky rice as carbon precursor, melamine as nitrogen source, and $Mg(OH)_2$ as template (Fig. 7a-c).[51] Their calculation results reveal that a nitrogen-free configuration with adjacent pentagon and heptagon carbon rings exhibits the lowest overpotential for both ORR and OER at the peak of volcano plot (Fig. 7d and e), which strongly supports aforementioned defect mechanism.[50] Alternatively, Tian and co-workers also developed a 3D porous graphene possessing high-level N-doping and rich structural defects (denoted as 3DNG-P) by a self-assembly hydrothermal approach and subsequent Ar plasma treatment.[55] They found the defective 3DNG-P can significantly improve the HER activity (achieving overpotential of 128 mV at 10 mA cm^{-2}) as compared to the sole N-doped counterpart, which are even comparable to those of some state-of-the-art transition-metal-based catalysts in HER.[55]

Most recently, Yu and co-workers successfully introduced N defects into g-C_3N_4 via an alkali-assisted (e.g. KOH) strategy during the thermal polymerization of nitrogen-rich precursors (e.g. urea).[56] They found that the N defect density increased with the ascending amount of KOH addition, evidenced by appearance of cyano groups (–C≡N) and diminishing peak of N-H bond in FTIR spectra (Fig. 8a). UV–vis diffuse reflectance spectra (DRS) revealed that a progressive red shift in the absorption edge was achieved with increasing KOH addition amount, indicating that N defects may induce narrowed bandgap of as-prepared g-C_3N_x samples (Fig. 8b). To better unveil the correlation between N defects and the narrowed bandgaps of g-C_3N_x samples, the author calculated the band structure and partial density of states (PDOS) for both defective g-C_3N_x and pristine g-C_3N_4 via density functional theory (DFT) (Fig. 8c-h).[56] The results reveal that the bandgap energy of defective g-C_3N_x decreases from 2.67 to 2.17 eV after introducing defects, which is attributed to the altered C2p and N2p orbitals in the conductive band of defective g-C_3N_x as compared to those of the pristine g-C_3N_4. All these experimental and theoretical results demonstrate that defects in carbon based materials plays a vital role in (photo)-eletrocatlaysis, which requires to unveil their catalytic mechanism urgently.

2.4 Defects enabling activated carbon to be "active"

The research above marked the initiation of defect mechanism. Besides the fundamental studies, one of our motivations is to produce efficient electrocatalysts for industrial applications in fuel cells and rechargeable metal-air batteries by a scalable and facile method. Generally, carbon materials, such as activated carbon (AC) is only used as a support for the catalysts because of its low catalytic activity, for example, the AC is not efficiently active for the electrochemical reactions even doped with nitrogen.[94] Due to the merits of AC in aspects of the low cost and the large scale production, if it can become active for electrocatalysis by applying the proposed defect mechanism, which will be a remarkable breakthrough to accelerate the practical applications of fuel cells.

Fig. 9a presents the schematic of the synthesis of defective activated carbon (D-AC) with unique defects for enhancing ORR performance by an easy N-doping and removal approach.[52] It can be seen that the resultant D-AC sample shows comparable ORR to the commercial Pt/C in an alkaline solution (Fig. 9b), and it is more stable than the Pt/C (Fig. 9c). Furthermore, rotation ring-disk electrode (RRDE) test (Fig. 9d) illustrates the low current density of ring disk in D-AC, indicating D-AC catalyst dominantly produces H_2O instead of H_2O_2, which can be attributed to the high electron transfer number of 3.6 in D-AC (close to 3.9 in commercial Pt/C) for ORR.[52]

Besides, the D-AC also shows improved HER activity (Fig. 9e) and good cyclic stability for the HER (Fig. 9f). As can be seen, the non-active activated carbon becomes an ideal catalyst for both the ORR and HER after a simple treatment based on the proposed defect mechanism. Apparently, this synthetic approach is possible for large scale production due to the low cost of the raw material, suggesting the D-AC has great potential for practical fuel cell and water splitting applications.

2.5 Coupling of defective carbons with non-noble metal species

In section 2.4, we present a kind of defective carbon (D-AC), which can be prepared from the cost effective activated carbon. Although the ORR performance of the D-AC is among the top of carbon based counterparts, it should be further enhanced, since it is still less active than the commercial Pt/C. It is reported that Mn–Co spinel could promote the ORR effectively,[95-97] and carbon support is also crucial to the ORR catalysts, so we used

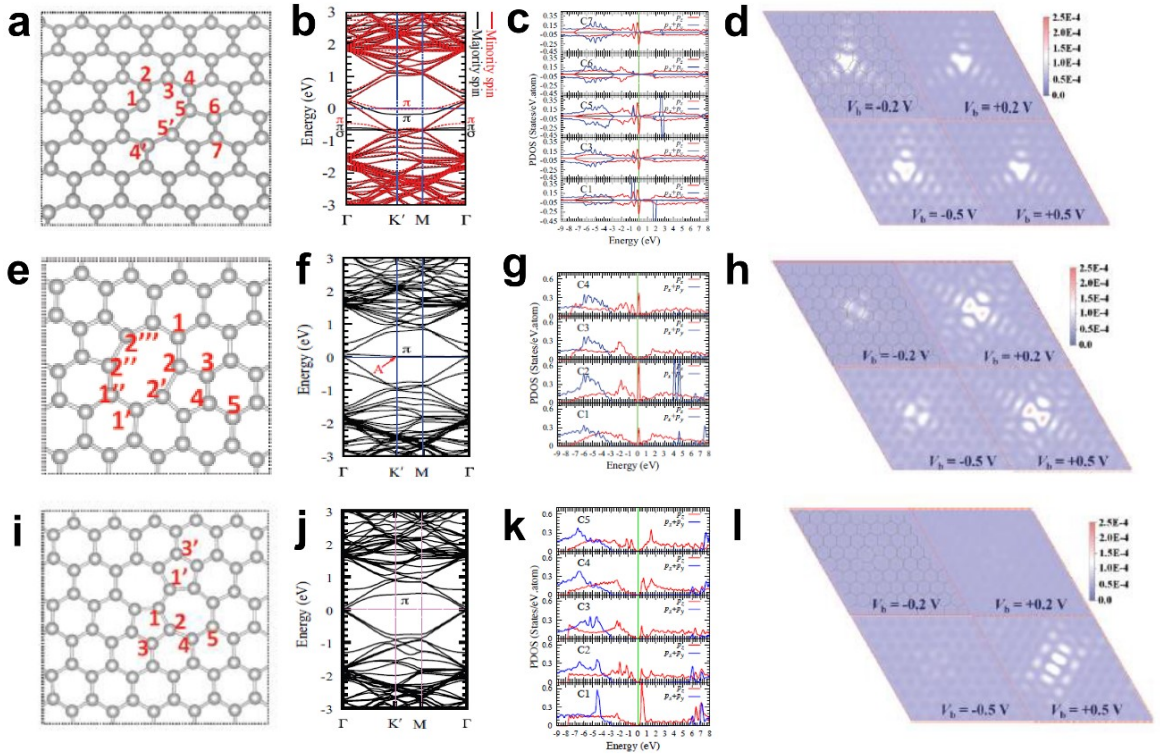

Fig. 11 Correlations of carbon defect types and electronic structures. a, e, i) Atomic structures of D59 (monovacancy, MV defect), D585 (divacancy, DV defect) and D5775 (Stone-Wales, SW defect). b, f, j) The band structures of graphene with MV, DV and SW. c, g, k) The partial density of states (PDOS) around defect region of MV, DV and SW. d, h, l) Simulated scanning tunnelling microscopy (STM) images for MV, DV and SW. Reproduced with permission.[93] Copyright 2013, American Physical Society.

the prepared D-AC as a support and loaded very low amount of $MnCo_2O_4$ spinel to further increase the ORR activity of the D-AC.[57] The D-AC supported $MnCo_2O_4$ sample (denoted as D-AC@2Mn-4Co) shows excellent ORR activity (comparable to commercial Pt/C catalyst), but the total metal content is lower than that of the Pt/C (13.4 *vs* 20 wt%), making it more appealing to practical fuel cell applications. Meanwhile, the D-AC@2Mn-4Co shows much higher durability than the Pt/C as well as resistance to the methanol crossover effect, implying its promising utilization for direct methanol fuel cells. We found that both the unique defects in the D-AC and the loaded $MnCo_2O_4$ spinel are essential to the outstanding ORR performance of the D-AC@2Mn-4Co, and the newly formed C-O-Mn/Co chemical bonds may play an important role in decreasing the reaction barrier and increasing the electron transfer efficiency during the ORR process. Very recently, we demonstrated a heterostructured NiFe LDH-NS@DG10 hybrid by coupling of exfoliated Ni–Fe layered double hydroxide (LDH) nanosheet (NS) and defective graphene (DG) as a bifunctional electrocatalyst for both OER and HER (Fig. 10a and b).[58] Impressively, this catalyst has exhibited high electrocatalytic overall watersplitting (20 mA cm^{-2} at 1.5 V) superior to those of NiFe LDH-NS@graphene (NG and G) counterparts (Fig. 10c and inset). It is remarkable that NiFe LDH-NS@DG ranks the best as compared to other non-noble metal bifunctional catalysts for overall alkaline water splitting (Fig. 10d), which can be easily driven by a 1.5 V solar panel (Fig. 10e). The simulation results further reveal that the formed heterostrucutre can efficiently enhance the charge separation and redistribution (electron-rich zones on carbon defect sites and electron-deficient zones on Ni–Fe LDH-NS) (Fig. 10f and g), thus facilitating the HER and OER conducted on defective graphene and NiFe LDH-NS, respectively (Fig. 10h).[58] Subsequently, Zhang and co-workers also demonstrated the direct ultilization of defects in carbon based materials to create atomic Co-N_x-C coordination structures, which can be served as bifunctional active sites for both ORR and OER.[59] Meanwhile, Zhang *et al.* directly identified the coordination structure of atmoic Ni trapped in graphene defects by using probe-corrected TEM, and further reveal that diffetent integrated coordination structures (atomic Ni at various carbon defects) may be the specific active sites for OER and HER, respectively.[60] For commercializing purpose, Liu *et al.* developed a controllable and scalable synthetic strategy of such defective carbons from cheap and earth-abundant bio-waste resources (e.g. seaweed), and the derived carbon based catalyst exhibited the efficent performance in both ORR and OER.[61]

Table 1 Summary of the defect density (n_D) and the corresponding ORR, OER or HER performance of our developed defective carbons.

Samples	I_D/I_G	$n_D\ (\mathrm{cm}^{-2})$	ORR $E_{1/2}$ (V *vs*. RHE)#	OER $E_{j=10}$ (V *vs*. RHE)*	HER $E_{j=10}$ (V *vs*. RHE)*	Ref.
PAF-C-700	0.81	2.28×10^{12}	0.56	-	-	48
PAF-C-800	0.84	2.38×10^{12}	0.57	-	-	48
PAF-C-900	0.85	2.41×10^{12}	0.68	-	-	48
PAF-C-1000	1.02	3.00×10^{12}	0.69	-	-	48
PC-I8-950	0.97	2.82×10^{12}	0.79	-	-	49
G	0.89	2.55×10^{12}	0.71	-	-0.42	50
NG	1.06	3.15×10^{12}	0.75	1.63	-0.35	50
DG	1.13	3.42×10^{12}	0.76	1.57	-0.15	50
H-AC	0.89	2.55×10^{12}	0.71	-	-0.63	52
N-AC	0.92	2.65×10^{12}	0.71	-	-0.60	52
D-AC	0.96	2.79×10^{12}	0.77	-	-0.51	52

$E_{1/2}$ is the ORR half-wave potential, * $E_{j=10}$ is the OER/HER potential obtained at the current density of 10 mA cm^{-2}. ORR is conducted in 0.1 M KOH, OER is conducted in 1 M KOH, and HER is conducted in 0.5 M H_2SO_4.

3. Mechanistic understanding on electronic structures of defective carbon based materials and electrocatalysis

3.1 Origin of carbon defect catalysis

In 2009, a new class of catalyst based on heteroatom-doped carbon materials was discovered, aiming to replace the platinum-based catalysts in fuel cells. Specifically, it is reported that nitrogen doped (N-doped) carbon nanotubes can act as efficient and robust catalysts in ORR.[27] Since then, massive efforts have been focused on the tailoring of carbon based electrochemical catalysts by heteroatoms doping/co-doping engineering (e.g. N, B, P and S).[4,5,30-34,62,63,98] Recently, these heteroatoms doped/co-doped carbon based catalysts have also been demonstrated to be efficient for OER and HER.[5,8,30-34,98] Despite great progress has been made on this topic, the origin of the electrocatalytic activity on heteroatom-doped carbon is still far from being clarified, which is actually the current research focus in this field.[55,99-104] For instance, in N-doped carbon based catalysts, it is still controversial whether the pyridinic or graphitic nitrogen is mainly responsible for the ORR. On the other hand, a large number of intrinsic structural and edge defects exist in the doped sp^2 carbon materials for accommodation of dopants, implying that local electronic structures may be significantly tuned by the synergistic effect of both dopants and defects, which leads to the generation of active sites for specific electrochemical reactions.[105] Therefore, the electrocatalytic activities of doped carbon materials should originate at least partially from the intrinsic defects. However, the research and knowledge of defect-induced electrocatalysis is still at very early stages to date which should be urgently developed.

Defects in carbon materials, especially vacant defects (e.g. pentagon, heptagon and octagon carbon rings), have been found to be capable of modifying the local atomic structure and tailoring its electronic environment.[91-93] For instance, it is theoretically predicted that a pentagon carbon ring will induce acceptor-like electronic states near the valence band, whereas a heptagon carbon ring will induce donor-like electronic states near the conduction band.[93] Intuitively, introducing topological defects into carbon based materials could break the delocalization orbitals of sp^2 carbon to create charged sites that may be favorable for the ORR, OER and HER.

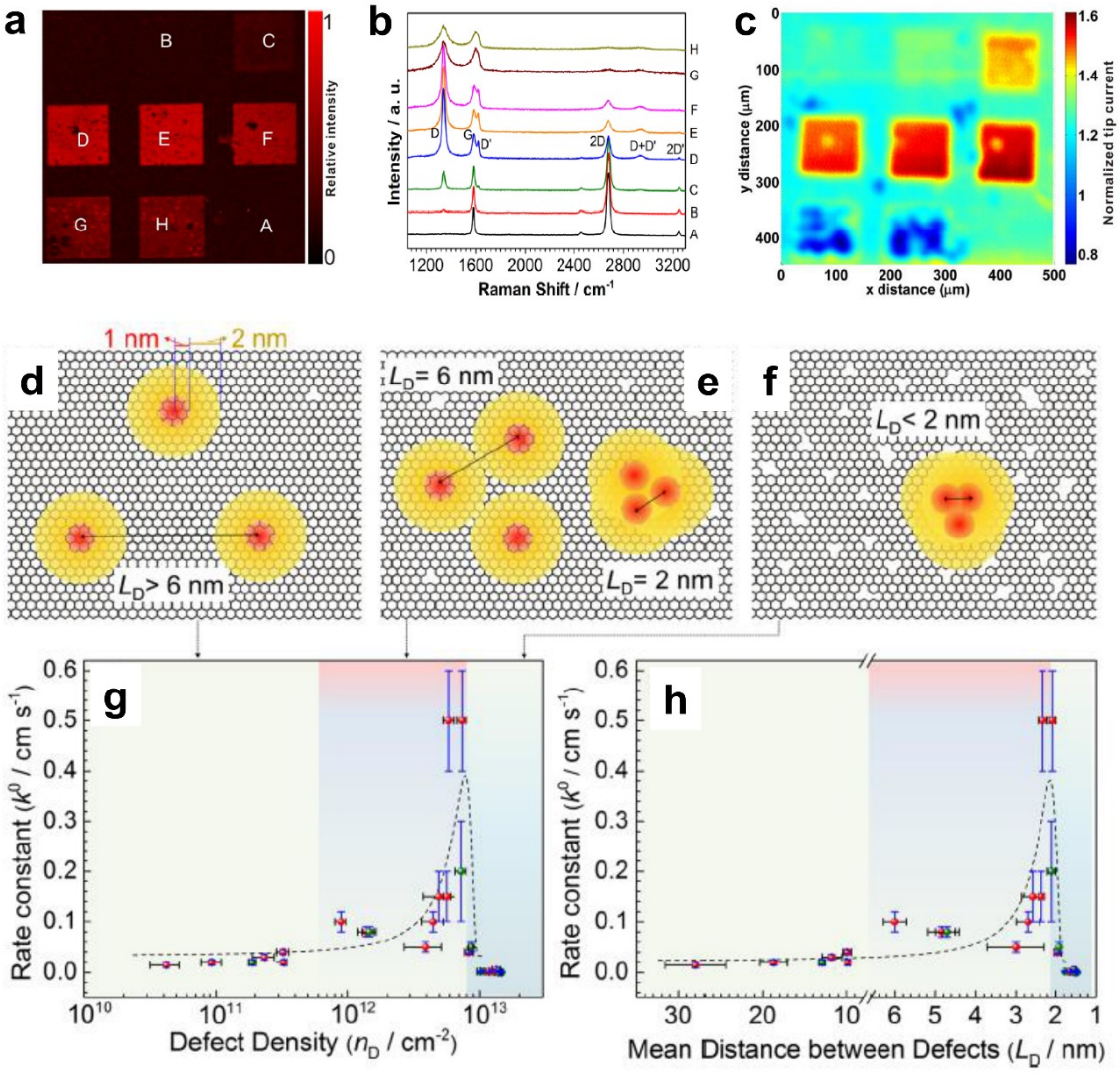

Fig. 12 Correlations of carbon defect density and heterogeneous electron transfer (HET) rate of graphene (pattern A: pristine graphene, pattern B to H: defective graphenes after Ar^+ radiation). a, b) Raman mapping of the D band of the defective graphene patterns and the corresponding Raman spectra. c) Scanning electrochemical microscopy (SECM) images of the same defective graphene patterns. d-f) The microscopic models in different defect density ranges (the red zone presents the structurally disordered area, and the yellow zone presents the electronically activated area): d) low defect density with L_D > 6 nm; e) moderate defect density with 2 nm ≤ L_D ≤ 6 nm; f) high defect density with L_D < 2 nm. g) The standard HET rate constant k^0 as a function of defect density n_D (cm^{-2}), and h) the mean distance between defects L_D (nm). Reproduced with permission.[118] Copyright 2014, American Chemical Society.

3.2 Correlations of carbon defect types and electronic structures

Generally, perfect graphene Fermi level (E_F) coincides well with Dirac point, and thus both the π and π^* bands near E_F are doubly degenerate. Interestingly, a recent theoretical study suggested that the electronic structures of graphene can be tuned by different local defects.[93] Specifically, three typical defects in graphene with associated electronic structures are investigated as shown in Fig. 11. D59 (adjacent hexagonal carbon rings with lacking of one carbon atom) and D585 are known as monovacancy (MV) defect (Fig. 11a) and divacancy (DV) defect (Fig. 11e) respectively, while D5775 (the combination of carbon rings with pentagon-heptagon-heptagon-pentagon) is a Stone-Wales (SW) defect associated with the reconstruction of a graphenic lattice without removal of carbon atoms (Fig. 11i). In Fig. 11b, the band structure of graphene with MV presents that E_F is below the Dirac point, indicating MV acts as a hole dopant. Furthermore, partial density of states (PDOS) of MV (Fig. 11c)

show that C1, C3, C5 and C7 have high defect π state densities derived from P_z orbitals around E_F where should be the active sites for electrocatalytic oxidation reactions. This result is consistent well with simulated scanning tunnelling microscopy (STM) image for MV (Fig. 11d), which shows slightly brighter domain around the MV under the negative bias voltages than that under the positive bias voltages, indicating p-type doping behaviour for the MV defect. In contrast, the band structures and PDOS for graphene with DV (Fig. 11f and g) and SW defects (Fig. 11j and k) present that the defect π states are both located above E_F, suggesting n-type doping behaviour in the DV and SW defects which appeals to electrocatalytic reduction reactions. As the defect level is unoccupied in DV and SW, the STM images with positive bias voltages have much brighter contrast than those with negative bias voltages (Fig. 11h and l), which is distinctly different from the case of MV where the defect π level is mostly below E_F.

3.3 Quantifying carbon defects for electrocatalysis

Quantifying defects in carbon based systems including a large family of *sp²* carbon structures, which is paramount to gain insight in their underlying mechanism for electrochemical applications.[106-108] Recently, extensive efforts have been made to study the relationship between the defects and disorder using Raman spectroscopy for nanographites,[109,110] amorphous carbons,[111,112] carbon nanotubes,[113] and graphene.[114-115] A quantitative formula has been proposed to correlate the mean distance between two adjacent defects ($\boldsymbol{L_D}$, nm) in graphene with the intensity ratio of the D band over G band ($\boldsymbol{I_D/I_G}$) in Raman spectra:

$$\frac{I_D}{I_G} = C_A \frac{(r_A^2 - r_S^2)}{(r_A^2 - 2r_S^2)} \left[e^{-\pi r_S^2/L_D^2} - e^{-\pi (r_A^2 - r_S^2)/L_D^2} \right] \quad (1)$$

where $\boldsymbol{r_s}$ and $\boldsymbol{r_A}$ are the radii of the "structurally disordered" area and the "activated" area surrounding the defect, respectively.[114] The factor $\boldsymbol{C_A}$ is defined by the electron-phonon matrix elements.[1117] It is demonstrated that the relationship between $\boldsymbol{C_A}$ and the incident laser energy ($\boldsymbol{E_L}$) can be defined by $\boldsymbol{C_A = (160 \pm 48) E_L^{-4}}$. For low-defect density regime ($\boldsymbol{L_D}$ > 10 nm), where $\boldsymbol{L_D > 2r_A}$, Eq. (1) can be approximated to be:

$$\frac{I_D}{I_G} \cong C_A \frac{\pi (r_A^2 - r_S^2)}{L_D^2} \quad (2)$$

By taking $\boldsymbol{r_A}$ = 3.1 nm, $\boldsymbol{r_s}$ = 1 nm, and if the excitation laser wavelength $\boldsymbol{\lambda_L}$ is in the visible light range, Eq. (2) can be rewritten as:

$$L_D^2 (nm^2) = (1.8 \pm 0.5) \times 10^{-9} \lambda_L^4 \left(\frac{I_D}{I_G}\right)^{-1} \quad (3)$$

The defect density ($\boldsymbol{n_D}$) can be calculated by $\boldsymbol{n_D(cm^{-2}) = 10^{14} / (\pi L_D^2)}$, therefore, Eq. (3) becomes:

$$n_D (cm^{-2}) = \frac{(1.8 \pm 0.5) \times 10^{22}}{\lambda_L^4} \left(\frac{I_D}{I_G}\right) \quad (4)$$

Therefore, we are able to deduce the defect densities of our developed defective carbons from $\boldsymbol{I_D/I_G}$ by using Eq. (4), and the results are summarized in Table 1. By comparing the calculated defect densities and observed electrochemical activities in ORR/OER/HER, it is indicated that we have succeeded in controlling different defect densities in our developed defective carbons, which is positive correlations to the catalytic performance in ORR/OER/HER.

Interestingly, it is notable that PC-I8-950 (no heteroatom-doping) with low defect density (2.82×10^{12} cm^{-2}) exhibits better ORR activity than that of PAF-C-1000 with high defect density (3.00×10^{12} cm^{-2}), suggesting the optimal electrochemical activity may need to be synergistically tuned by defect density and other factors such as conductivity and nanostructure.

To further investigate the influence of carbon defect density on the electrochemical activity, a series of Ar^+ radiated graphene samples (eliminating doping effect) with precise control of defect densities are characterized by Raman spectroscopy and scanning electrochemical microscopy (SECM) as shown in Fig. 12.[118] Fig. 11a presents Raman mapping of the D band of the defective graphene (from pattern B to H) and pristine graphene (pattern A), which shows that the intensity of the D band increases from pattern B to E followed by an intensity decreasing from pattern F to H. This result is simultaneously evidenced by the corresponding Raman spectra in Fig. 12b. Subsequently, to evaluate the electrochemical activities of the above defective graphene samples, SECM is applied to determine heterogeneous electron transfer (HET) rates. As shown in Fig. 12c, it is observed that with increasing defect density, the tip current firstly increases (from pattern B to H) then decreases (pattern G to H) to even below that of the pristine graphene (pattern A). The two-stage SECM patterns are in agreement with the Raman D-band mapping results, which indicates the electrochemical activity of single layer graphene is relied on its defect density. To get insight into defects in graphene, three microscopic models in different defect density ranges (the red zone presents the structurally disordered area, and the yellow zone presents the electronically activated area) are established (Fig. 12d-f). In the case of low defect density (Fig. 12d), the carbon defects exist independently and sparsely. With the increase of defect density, the activated areas of defects appear to overlap, leading to enhancement of density of states at overlapped defects (Fig. 12e and f). However, it is also remarkable that the electron transport capability (conductivity) in defective graphene with the high defect density will drop with the significant loss of the perfect sp^2 lattice.[106] The quantitative correlations between defect density (mean distance between defects) and electrochemical activities

are presented in Fig. 12g and h, which demonstrate that a moderate defect density range is optimal for electrochemical performance.

Based on above review of correlations between electronic structures and electrocatalysis in defective carbons, it can be concluded that two main factors (defect types and defect density) are crucial to the specific electrochemical activities (ORR, OER and HER) in carbon based electrocatalysts.

4. Conclusive remarks and prospects

Carbon-based materials feature unique advantages for designated catalysis due to their various merits. However, to date, the electrochemical activities of these electrocatalysts are usually attributed to different active dopants (e.g., N, B, P or S), whereas the contribution of intrinsic/induced carbon defects has often been neglected. Recently, studies on defects-promoted electrochemical reactions has been a hot topic, and is now gaining increasing research attention. In particular, a series of recently reported defective carbon based materials showcase excellent electrochemical activities in ORR, OER and HER. More importantly, a defect catalysis mechanism originating from both defect types and defect density is introduced in this review, which may provide the guidance to the proof-of-concept atomic design of highly active electrocatalysts for diverse applications in energy conversion and storage.

Although great advance has been made in the design of defective carbon based materials as newly efficient and robust electrocatalysts by combining the currently available computational and experimental methods, there are still several critical challenges that are not addressed yet: (1) it is difficult to precisely control the defect types in carbons by current thermal treatments or direct radiation methods, leading to low selectivity to specific electrochemical reactions; (2) correlation analysis between defect density and electrocatalytic activity is still lacking in the present development stage of defective carbon based catalysts for ORR, OER or HER; (3) despite defective carbons exhibit significant enhancement in ORR (e.g. D-AC comparable to Pt/C) and OER (e.g. DG comparable to Ir/C) in alkaline, their electrochemical performance still need further improvement due to inferior to Pt based benchmarking catalyst in more broad applications such as ORR in acidic condition.

In conclusion, the future directions of catalyst development for defect chemistry in electrocatalysis should be focused on the following aspects: (1) new synthetic strategies must be developed to experimentally precise control of defect type for only enhancing one specific electrochemical reaction without side effect, which is difficult but important to identify the real active sites of defects (e.g. N-removal from specific types of N dopants); (2) quantitatively optimising electrocatalytic activity by balancing the defect density induced increase of density of states (DOS) and decrease of conductivity in defective carbons; (3) utilization of defect sites in defective carbons for efficiently and largely anchoring metallic dopants at atomic level, which could open a new venue toward single-atom catalysis (a new research frontier in heterogeneous catalysis); and (4) cost-effective large-scale production of tailor-made defective carbon based catalysts is necessary for industrial applications. Prospectively, it is no doubt that continued research and development in this exciting field should result in improved fuel economy and decreased harmful emissions.

Acknowledgements

We thank the financial support from Australian Research Council (ARC DP170103317 and DP170102267). Y. J. also thanks the ARC Discovery Early Career Researcher Award (ARC DE180101030).

Notes and references

1 R. Bashyam, P. Zelenay, *Nature*, 2006, **443**, 63.
2 G. Wu, K. L. More, C. M. Johnston, P. Zelenay, *Science*, 2011, **332**, 443.
3 N. Yamada, T. Yaguchi, H. Otsuka, M. Sudoh, *J. Electrochem. Soc.*, 1999, **146**, 2587.
4 L. M. Dai, Y. H. Xue, L. T. Qu, H. J. Choi, J. B. Baek, *Chem. Rev.*, 2015, **115**, 4823.
5 J. T. Zhang, Z. H. Zhao, Z. H. Xia, L. M. Dai, *Nat. Nanotechnol.*, 2015, **10**, 444.
6 Y. G. Li, H. J. Dai, *Chem. Soc. Rev.*, 2014, **43**, 5257.
7 Y. Jiao, Y. Zheng, M. T. Jaroniec, S. Z. Qiao, *Chem. Soc. Rev.*, 2015, **44**, 2060.
8 X. X. Zou, Y. Zhang, *Chem. Soc. Rev.*, 2015, **44**, 5148.
9 Y. Y. Liang, Y. G. Li, H. L. Wang, H. J. Dai, *J. Am. Chem. Soc.*, 2013, **135**, 2013.
10 Y. Y. Liang, Y. G. Li, H. L. Wang, J. G. Zhou, J. Wang, T. Regier, H. J. Dai, *Nat. Mater.*, 2011, **10**, 780.
11 S. Cobo, J. Heidkamp, P. A. Jacques, J. Fize, V. Fourmond, L. Guetaz, B. Jousselme, V. Ivanova, H. Dau, S. Palacin, M. Fontecave, V. Artero, *Nat. Mater.*, 2012, **11**, 802.
12 H. Y. Jin, J. Wang, D. F. Su, Z. Z. Wei, Z. F. Pang, Y. Wang, *J. Am. Chem. Soc.*, 2015, **137**, 2688.
13 M. Gong, Y. G. Li, H. L. Wang, Y. Y. Liang, J. Z. Wu, J. G. Zhou, J. Wang, T. Regier, F. Wei, H. J. Dai, *J. Am. Chem. Soc.*, 2013, **135**, 8452.
14 E. J. Popczun, J. R. McKone, C. G. Read, A. J. Biacchi, A. M. Wiltrout, N. S. Lewis, R. E. Schaak, *J. Am. Chem. Soc.*, 2013, **135**, 9267.
15 R. D. L. Smith, M. S. Prevot, R. D. Fagan, S. Trudel, C. P. Berlinguette, *J. Am. Chem. Soc.*, 2013, **135**, 11580.
16 Y. F. Xu, M. R. Gao, Y. R. Zheng, J. Jiang, S. H. Yu, *Angew. Chem.-Int. Edit.*, 2013, **52**, 8546.
17 M. Gong, W. Zhou, M. C. Tsai, J. G. Zhou, M. Y. Guan, M. C. Lin, B. Zhang, Y. F. Hu, D. Y. Wang, J. Yang, S. J. Pennycook, B. J. Hwang, H. J. Dai, *Nat. Commun.*, 2014, **5**, 6.
18 X. Huang, C. L. Tan, Z. Y. Yin, H. Zhang, *Adv. Mater.*, 2014, **26**, 2185.
19 R. Lv, J. A. Robinson, R. E. Schaak, D. Sun, Y. F. Sun, T. E. Mallouk, M. Terrones, *Accounts Chem. Res.*, 2015, **48**, 56.
20 C. C. L. McCrory, S. Jung, I. M. Ferrer, S. M. Chatman, J. C. Peters, T. F. Jaramillo, *J. Am. Chem. Soc.*, 2015, **137**, 4347.
21 Y. G. Li, H. L. Wang, L. M. Xie, Y. Y. Liang, G. S. Hong, H. J. Dai, *J. Am. Chem. Soc.*, 2011, **133**, 7296.
22 T. F. Jaramillo, K. P. Jorgensen, J. Bonde, J. H. Nielsen, S. Horch, I. Chorkendorff, *Science*, 2007, **317**, 100.

23 J. H. Wang, W. Cui, Q. Liu, Z. C. Xing, A. M. Asiri, X. P. Sun, *Adv. Mater.*, 2016, **28**, 215.
24 J. Liang, R. F. Zhou, X. M. Chen, Y. H. Tang, S. Z. Qiao, *Adv. Mater.*, 2014, **26**, 6074.
25 P. W. Du, R. Eisenberg, *Energy Environ. Sci.*, 2012, **5**, 6012.
26 S. Najmaei, Z. Liu, W. Zhou, X. L. Zou, G. Shi, S. D. Lei, B. I. Yakobson, J. C. Idrobo, P. M. Ajayan, J. Lou, *Nat. Mater.*, 2013, **12**, 754.
27 K. P. Gong, F. Du, Z. H. Xia, M. Durstock, L. M. Dai, *Science*, 2009, **323**, 760.
28 Y. Zheng, Y. Jiao, J. Chen, J. Liu, J. Liang, A. Du, W. M. Zhang, Z. H. Zhu, S. C. Smith, M. Jaroniec, G. Q. Lu, S. Z. Qiao, *J. Am. Chem. Soc.*, 2011, **133**, 20116.
29 Y. Zhao, R. Nakamura, K. Kamiya, S. Nakanishi, K. Hashimoto, *Nat. Commun.*, 2013, **4**, 7.
30 Y. Zheng, Y. Jiao, L. H. Li, T. Xing, Y. Chen, M. Jaroniec, S. Z. Qiao, *ACS Nano*, 2014, **8**, 5290.
31 C. G. Hu, L. M. Dai, Angew. Chem.-Int. Edit., 2016, 55, 11736.
32 Y. X. Fang, X. C. Wang, *Angew. Chem.-Int. Edit.*, 2017, **56**, 15506.
33 X. E. Liu, L. M. Dai, *Nat. Rev. Mater.*, 2016, **1**, 16064.
34 J. T. Zhang, L. T. Qu, G. Q. Shi, J. Y. Liu, J. F. Chen, L. M. Dai, *Angew. Chem.-Int. Edit.*, 2016, **55**, 2230.
35 H. H. Ou, P. J. Yang, L. H. Lin, M. Anpo, X. C. Wang, *Angew. Chem. Int. Ed.*, 2017, **56**, 10905.
36 C. Yang, B. Wang, L. Z. Zhang, L. Yin, X. C. Wang, *Angew. Chem. Int. Ed.*, 2017, **56**, 6627.
37 H. H. Ou, L. H. Lin, Y. Zheng, P. J. Yang, Y. X. Fang, X. C. Wang, *Adv. Mater.*, 2017, **29**, 1700008.
38 P. J. Yang, H. H. Ou, Y. X. Fang, X. C. Wang, *Angew. Chem. Int. Ed.*, 2017, **56**, 3992.
39 F. S. Guo, P. J. Yang, Z. M. Pan, X. N. Cao, Z. L. Xie, X. C. Wang, *Angew. Chem. Int. Ed.*, 2017, **56**, 8231.
40 Y. X. Fang, X. C. Wang, *Angew. Chem. Int. Ed.*, 2017, **56**, 15506.
41 M. Z. Rahman, J. Zhang, Y. Tang, K. Davey, S. Qiao, *Mater. Chem. Front.* 2017, **1**, 562.
42 A. Eftekhari, Z. Fan, *Mater. Chem. Front.* 2017, **1**, 1001.
43 K. Zhu, Y. Wang, J. Tang, S. Guo, Z. Gao, Y. Wei, G. Chen, Y. Gao, *Mater. Chem. Front.* 2017, **1**, 958.
44 K. Yuan, T. Hu, Y. Xu, R. Graf, L. Shi, M. Forster, T. Pichler, T. Riedl, Y. Chen, U. Scherf, *Mater. Chem. Front.* 2017, **1**, 278.
45 L. J. Yang, S. J. Jiang, Y. Zhao, L. Zhu, S. Chen, X. Z. Wang, Q. Wu, J. Ma, Y. W. Ma, Z. Hu, *Angew. Chem.-Int. Edit.*, 2011, **50**, 7132.
46 J. P. Paraknowitsch, A. Thomas, *Energy Environ. Sci.*, 2013, **6**, 2839.
47 Y. Zhao, L. J. Yang, S. Chen, X. Z. Wang, Y. W. Ma, Q. Wu, Y. F. Jiang, W. J. Qian, Z. Hu, *J. Am. Chem. Soc.*, 2013, **135**, 1201.
48 H. Y. Zhao, C. H. Sun, Z. Jin, D. W. Wang, X. C. Yan, Z. G. Chen, G. S. Zhu and X. D. Yao, *J. Mater. Chem. A*, 2015, **3**, 11736.
49 X. J. Zhao, X. Q. Zou, X. C. Yan, C. L. Brown, Z. G. Chen, G. S. Zhu, X. D. Yao, *Inorg. Chem. Front.*, 2016, **3**, 417.
50 Y. Jia, L. Z. Zhang, A. J. Du, G. P. Gao, J. Chen, X. C. Yan, C. L. Brown, X. D. Yao, *Adv. Mater.*, 2016, **28**, 9532.
51 C. Tang, H. F. Wang, X. Chen, B. Q. Li, T. Z. Hou, B. S. Zhang, Q. Zhang, M. M. Titirici, F. Wei, *Adv. Mater.*, 2016, **28**, 6845.
52 X. C. Yan, Y. Jia, T. Odedairo, X. J. Zhao, Z. Jin, Z. H. Zhu, X. D. Yao, *Chem. Commun.*, 2016, **52**, 8156.
53 Y. Jiang, L. Yang, T. Sun, J. Zhao, Z. Lyu, O. Zhuo, X. Wang, Q. Wu, J. Ma, Z. Hu, *ACS Catal.*, 2015, **5**, 6707.
54 L. Tao, Q. Wang, S. Dou, Z. Ma, J. Huo, S. Wang, L. Dai, *Chem. Commun.*, 2016, **52**, 2764.
55 Y. Tian, Y. F. Ye, X. J. Wang, S. Peng, Z. Wei, X. Zhang, W. M. Liu, *Appl. Catal. A*, 2016, **529**, 127.
56 H. J. Yu, R. Shi, Y. X. Zhao, T. Bian, Y. F. Zhao, C. Zhou, G. I. N. Waterhouse, L. Z. Wu, C. H. Tung, T. R. Zhang, *Adv. Mater.*, 2017, **29**, 1605148.
57 X. C. Yan, Y. Jia, J. Chen, Z. H. Zhu and X. D. Yao, *Adv. Mater.*, 2016, **28**, 8771.
58 Y. Jia, L. Z. Zhang, G. P. Gao, H. Chen, B. Wang, J. Z. Zhou, M. T. Soo, M. Hong, X. C. Yan, G. R. Qian, J. Zou, A. J. Du, X. D. Yao, *Adv. Mater.*, 2017, **29**, 1700017.
59 C. Tang, B. Wang, H. F. Wang, Q. Zhang, *Adv. Mater.*, 2017, **29**, 1703185.
60 L. Z. Zhang, Y. Jia, G. P. Gao, X. C. Yan, N. Chen, J. Chen, M. T. Soo, B. Wood, D. J. Yang, A. Du, X. D. Yao, *Chem*, 2018, **4**, 285.
61 L. Liu, X. Yang, N. Ma, H. Liu, Y. Xia, C. Chen, D. J. Yang, X. D. Yao, *Small*, 2016, **12**, 1295.
62 H. B. Yang, J. W. Miao, S. F. Hung, J. Z. Chen, H. B. Tao, X. Z. Wang, L. P. Zhang, R. Chen, J. J. Gao, H. M. Chen, L. M. Dai, B. Liu, *Sci. Adv.*, 2016, **2**, 11.
63 D. H. Guo, R. Shibuya, C. Akiba, S. Saji, T. Kondo, J. Nakamura, *Science*, 2016, **351**, 361.
64 S. Kundu, T. C. Nagaiah, W. Xia, Y. M. Wang, S. V. Dommele, J. H. Bitter, M. Santa, G. Grundmeier, M. Bron, W. Schuhmann, M. J. Muhler, *Phys. Chem. C*, 2009, **113**, 14302.
65 H. B. Li, W. J. Kang, L. Wang, Q. L. Yue, S. L. Xu, H. S. Wang, J. F. Liu, *Carbon*, 2013, **54**, 249.
66 C. V. Rao, C. R. Cabrera, Y. J. Ishikawa, *Phys. Chem. Lett.*, 2010, **1**, 2622.
67 K. A. Kurak, A. B. Anderson, *J. Phys. Chem. C*, 2009, **113**, 6730.
68 J. Yan, H. Meng, F. Y. Xie, X. L. Yuan, W. D. Yu, W. R. Lin, W. P. Ouyang, D. S. Yuan, *J. Power Sources*, 2014, **245**, 772.
69 M. Park, T. Lee, B. S. Kim, *Nanoscale*, 2013, **5**, 12255.
70 S. Yasuda, L. Yu, J. Kim, K. Murakoshi, *Chem. Commun.*, 2013, **49**, 9627.
71 D. Guo, R. Shibuya, C. Akiba, S. Saji, T. Kondo, J. Nakamura *Science*, 2016, **351**, 6271.
72 L. Qu, Y. Liu, J. B. Baek, L. M. Dai, *ACS Nano*, 2010, **4**, 1321.
73 R. L. Liu, D. Q. Wu, X. L. Feng, K. Mullen, *Angew. Chem. Int. Ed.*, 2010, **49**, 2565.
74 H. Niwa, K. Horiba, Y. Harada, M. Oshima, T. Ikeda, K. Terakura, J. Ozaki, S. Miyata, *J. Power Sources*, 2009, **187**, 93.
75 D. S. Geng, Y. Chen, Y. G. Chen, Y. L. Li, R. Y. Li, X. L. Sun, S. Y. Ye, S. Knights, *Energy Environ. Sci.*, 2011, **4**, 760.
76 B. Zheng, J. Wang, F. B. Wang, X. H. Xia, *Electrochem. Commun.*, 2013, **28**, 24.
77 Z. Y. Lin, G. H. Waller, Y. Liu, M. L. Liu, C. P. Wong, *Nano Energy*, 2013, **2**, 241.
78 Y. Lei, L. Wei, S. Zhai, Y. Wang, H. E. Karahan, X. Chen, Z. Zhou, C. Wang, X. Sui, Y. Chen, *Mater. Chem. Front.*, 2018, **2**, 102.
79 W. Wei, H. W. Liang, K. Parvez, X. D. Zhuang, X. L. Feng, K. Mullen, *Angew. Chem.-Int. Edit.*, 2014, **53**, 1570.
80 S. Chen, J. Y. Bi, Y. Zhao, L. J. Yang, C. Zhang, Y. W. Ma, Q. Wu, X. Z. Wang, Z. Hu, *Adv. Mater.*, 2012, **24**, 5593.
81 Z. H. Sheng, L. Shao, J. J. Chen, W. J. Bao, F. B. Wang, X. H. Xia, *ACS Nano*, 2011, **5**, 4350.
82 I. Y. Jeon, D. S. Yu, S. Y. Bae, H. J. Choi, D. W. Chang, L. M. Dai, J. B. Baek, *Chem. Mat.*, 2011, **23**, 3987.
83 D. S. Geng, Y. Chen, Y. G. Chen, Y. L. Li, R. Y. Li, X. L. Sun, S. Y. Ye, S. Knights, *Energy Environ. Sci.*, 2011, **4**, 760.
84 P. Chen, T. Y. Xiao, Y. H. Qian, S. S. Li, S. H. Yu, *Adv. Mater.*, 2013, **25**, 3192.
85 Z. J. Wang, R. R. Jia, J. F. Zheng, J. G. Zhao, L. Li, J. L. Song, Z. P. Zhu, *ACS Nano*, 2011, **5**, 1677.
86 Y. Kim, J. Ihm, E. Yoon, G. D. Lee, *Phys. Rev. B*, 2011, **84**, 5.
87 M. M. Ugeda, I. Brihuega, F. Hiebel, P. Mallet, J. Y. Veuillen, J. M. Gomez-Rodriguez, F. Yndurain, *Phys. Rev. B*, 2012, **85**, 5.
88 A. Aijaz, N. Fujiwara, Q. Xu, *J. Am. Chem. Soc.*, 2014, **136**, 6790.
89 W. Xia, A. Mahmood, R. Q. Zou, Q. Xu, *Energy Environ. Sci.*, 2015, **8**, 1837.
90 L. Zhang, Q. Xu, J. Niu, Z. Xia, *Phys. Chem. Chem. Phys.* 2015, **17**, 16733.
91 J. Kotakoski, A. V. Krasheninnikov, U. Kaiser, J. C. Meyer, *Phys. Rev. Lett.*, 2011, **106**, 4.

92 F. Banhart, J. Kotakoski, A. V. Krasheninnikov, *ACS Nano*, 2011, **5**, 26.
93 Z. F. Hou, X. L. Wang, T. Ikeda, K. Terakura, M. Oshima, M. Kakimoto, *Phys. Rev. B*, 2013, **87**, 16.
94 B. Zhang, Z. H. Wen, S. Q. Ci, S. Mao, J. H. Chen, Z. He, *ACS Appl. Mater. Interfaces*, 2014, **6**, 7464.
95 F. Y. Cheng, J. A. Shen, B. Peng, Y. D. Pan, Z. L. Tao, *J. Chen, Nat. Chem.*, 2011, **3**, 79.
96 Y. Y. Liang, H. L. Wang, J. G. Zhou, Y. G. Li, J. Wang, T. Regier, H. J. Dai, *J. Am. Chem. Soc.*, 2012, **134**, 3517.
97 C. Li, X. P. Han, F. Y. Cheng, Y. X. Hu, C. C. Chen, J. Chen, *Nat. Commun.*, 2015, **6**, 8.
98 Y. Zheng, Y. Jiao, Y. H. Zhu, L. H. Li, Y. Han, Y. Chen, A. J. Du, M. Jaroniec, S. Z. Qiao, *Nat. Commun.*, 2014, **5**, 8.
99 L. T. Qu, Y. Liu, J. B. Baek, L. M. Dai, *ACS Nano*, 2010, **4**, 1321.
100 L. P. Zhang, Z. H. Xia, *J. Phys. Chem. C*, 2011, **115**, 11170.
101 L. F. Lai, J. R. Potts, D. Zhan, L. Wang, C. K. Poh, C. H. Tang, H. Gong, Z. X. Shen, L. Y. Jianyi, R. S. Ruoff, *Energy Environ. Sci*., 2012, **5**, 7936.
102 W. Ding, Z. D. Wei, S. G. Chen, X. Q. Qi, T. Yang, J. S. Hu, D. Wang, L. J. Wan, S. F. Alvi, L. Li, *Angew. Chem.-Int. Edit*., 2013, **52**, 11755.
103 H.-W. Liang, X. Zhuang, S. Bruller, X. Feng, K. Mullen, *Nat. Commun*., 2014, **5**, 4973.
104 T. Xing, Y. Zheng, L. H. Li, B. C. C. Cowie, D. Gunzelmann, S. Z. Qiao, S. M. Huang, Y. Chen, *ACS Nano*, 2014, **8**, 6856.
105 D. C. Wei, Y. Q. Liu, Y. Wang, H. L. Zhang, L. P. Huang, G. Yu, *Nano Lett*., 2009, **9**, 1752.
106 J. H. Chen, W. G. Cullen, C. Jang, M. S. Fuhrer, E. D. Williams, *Phys. Rev. Lett.*, 2009, **102**, 4.
107 C. R. Dean, A. F. Young, I. Meric, C. Lee, L. Wang, S. Sorgenfrei, K. Watanabe, T. Taniguchi, P. Kim, K. L. Shepard, J. Hone, *Nat. Nanotechnol.*, 2010, **5**, 722.
108 Z. H. Ni, L. A. Ponomarenko, R. R. Nair, R. Yang, S. Anissimova, I. V. Grigorieva, F. Schedin, P. Blake, Z. X. Shen, E. H. Hill, K. S. Novoselov, A. K. Geim, *Nano Lett*., 2010, **10**, 3868.
109 L. G. Cancado, A. Jorio, M. A. Pimenta, *Phys. Rev. B*, 2007, **76**, 7.
110 M. A. Pimenta, G. Dresselhaus, M. S. Dresselhaus, L. G. Cancado, A. Jorio, R. Saito, *Phys. Chem. Chem. Phys*., 2007, **9**, 1276.
111 A. C. Ferrari, J. Robertson, *Phys. Rev. B*, 2000, **61**, 14095.
112 A. C. Ferrari, S. E. Rodil, J. Robertson, *Phys. Rev. B*, 2003, **67**, 20.
113 M. S. Dresselhaus, G. Dresselhaus, R. Saito, A. Jorio, *Phys. Rep.-Rev. Sec. Phys. Lett.* 2005, **409**, 47.
114 L. G. Cancado, A. Jorio, E. H. M. Ferreira, F. Stavale, C. A. Achete, R. B. Capaz, M. V. O. Moutinho, A. Lombardo, T. S. Kulmala, A. C. Ferrari, *Nano Lett.*, 2011, **11**, 3190.
115 A. C. Ferrari, *Solid State Commun*., 2007, **143**, 47.
116 A. C. Ferrari, D. M. Basko, *Nat. Nanotechnol.*, 2013, **8**, 235.
117 M. M. Lucchese, F. Stavale, E. H. M. Ferreira, C. Vilani, M. V. O. Moutinho, R. B. Capaz, C. A. Achete, A. Jorio, *Carbon*, 2010, **48**, 1592.
118 J. H. Zhong, J. Zhang, X. Jin, J. Y. Liu, Q. Y. Li, M. H. Li, W. W. Cai, D. Y. Wu, D. P. Zhan, B. Ren, *J. Am. Chem. Soc.*, 2014, **136**, 16609.